DOE/PC/92190--T8

PSI-1178/05/95

FUNDAMENTAL STUDY OF ASH FORMATION AND DEPOSITION: EFFECT OF REDUCING STOICHIOMETRY

Quarterly Report No. 8
for the Period 1 January to 31 March 1995

L.E. Bool III and J.J. Helble
PSI Technologies

A.F. Sarofim and Taofang Zeng
Massachusetts Institute of Technology

T.W. Peterson and D. Gallien
University of Arizona

and

N. Shah, G.P. Huffman, F.E. Huggins, A. Shah, and K.R.P.M. Rao
University of Kentucky

Editor:
Dr. J.J. Helble
PSI Technologies

DATE PUBLISHED - May 1995

Prepared under
DoE Contract No. DE-AC22-93PC92190

U.S. DEPARTMENT OF ENERGY
Pittsburgh Energy Technology Center
P.O. Box 10940
Pittsburgh, PA 15236

PSI
PHYSICAL SCIENCES INC.
20 New England Business Center ▮ Andover, MA 01810-1077 ▮ U.S.A.

PSI-1178 /05/95

FUNDAMENTAL STUDY OF ASH FORMATION AND DEPOSITION: EFFECT OF REDUCING STOICHIOMETRY

Quarterly Report No. 8
for the Period 1 January to 31 March 1995

L.E. Bool III and J.J. Helble
PSI Technologies

A.F. Sarofim and Taofang Zeng
Massachusetts Institute of Technology

T.W. Peterson and D. Gallien
University of Arizona

and

N. Shah, G.P. Huffman, F.E. Huggins, A. Shah, and K.R.P.M. Rao
University of Kentucky

Editor:
Dr. J.J. Helble
PSI Technologies

DATE PUBLISHED - May 1995

Prepared under
DoE Contract No. DE-AC22-93PC92190

U.S. DEPARTMENT OF ENERGY
Pittsburgh Energy Technology Center
P.O. Box 10940
Pittsburgh, PA 15236

MASTER

DISCLAIMER

Portions of this document may be illegible in electronic image products. Images are produced from the best available original document.

TABLE OF CONTENTS

LIST OF ILLUSTRATIONS

SECTION 1

EXECUTIVE SUMMARY

1. EXECUTIVE SUMMARY

The technical objectives of this project are:

a: To identify the partitioning of inorganic coal constituents among vapor, submicron fume, and fly ash products generated during the combustion of pulverized coal under a variety of combustion conditions. Fuel lean and fuel rich combustion conditions will be considered.

b: To identify and quantify the fundamental processes by which the transformations of minerals and organically-associated inorganic species occurs. Emphasis will be placed on identifying any changes that occur as a result of combustion under sub-stoichiometric combustion conditions.

c: To incorporate the effects of combustion stoichiometry into an Engineering Model for Ash Formation based upon the understanding developed in (a) and (b). When completed, this model will predict the particle size and chemical composition distributions of ash formed during the combustion of pulverized coal under a broad range of conditions.

A description of the work plan for accomplishing these objectives is presented in Section 2 of this report.

The work discussed in this report highlights the accomplishments of the eighth quarter of this two year project. This includes reporting of: University of Kentucky Mössbauer and XAFS analyses of ash samples generated by PSIT, by DOE/PETC in the DOE fuels evaluation furnace, and by the utility PowerGen in the Ratcliffe U.K power generating station; M.I.T.'s continuing evaluation of the fate of iron as a function of combustion stoichiometry; UA's continuing modifcation of the self-sustained combustion furnace; PSIT's analysis of coal and ash data provided to this program by Imperial College, and further development of PSIT's Engineering Model for Ash Formation (EMAF).

In Section 3 of this report, further analysis of coal and ash data obtained by Imperial College is discussed. As part of a collaboration with the investigators of this program, the members of a large-scale combustion program in the U.K., led by the utility Powergen, have provided coal, ash, and deposit samples to this program. In addition, the group at Imperial College has analyzed one of the Pittsburgh #8 coals studied in this DOE program; in Section 3, the results of this analysis are compared with U. Kentucky analyses obtained previously. The mineral size distribution for the washed Pittsburgh #8 coal measured by CCSEM at Imperial College was in excellent agreement with an earlier measurement of the same sample by the University of Kentucky. Analyses of the Silverdale coal were qualitatively consistent, showing some disagreement in the smaller mineral size fractions. Because the two coal samples were not identical, we cannot conclude whether the differences resulted from analytical differences or small differences in the coal samples themselves. It should be noted that mineral composition distributions were in excellent agreement.

In Section 4 of this report, the results of recent analytical work by the University of Kentucky are presented. Data obtained from initial Mössbauer and Ca XAFS analysis of ash samples obtained from combustion of Silverdale coal in the Ratcliffe (U.K.) power station are presented. Samples generated from combustion under low-NOx firing conditions at three different excess oxygen levels were provided to PSIT by Imperial College; to date, only those obtained at the lowest excess oxygen level of 2.5% have been analyzed by the University of Kentucky. Comparing probe deposit, fly ash, and bottom ash samples for forms of iron, the probe deposit samples had the highest concentrations of iron in glassy phases, whereas the bottom ash had the lowest. The Fe(+2)/Fe(+3) ratio for glassy phase iron also increased in the series bottom ash - fly ash - probe deposit ash. Interestingly, the inner layers on the deposit probe had lower concentrations of glass-phase iron than did the bulk deposit. This suggests that either (a) very low levels of glass-phase iron are sufficient to form an initial deposit on the probe surface, or (2) the low metal temperatures of the air-cooled probe caused iron to crystallize out of the glassy melt in the inner layers. Ca XANES data obtained for these samples show no differences from sample to sample.

Also reported in Section 4 are the Mössbauer and Ca XANES analytical results for (1) samples generated (under separate support provided by Brookhaven Laboratories) in the in-situ XAFS combustor test facility using Silverdale coal, and (2) samples generated in the PETC pilot scale combustion test furnace using a washed Pittsburgh #8 coal similar to the one examined in this program. The latter samples indicated that iron transformations were completed within the first 1.7 s residence time in the system.

In Section 5, recent MIT efforts in modeling iron transformations during combustion are discussed.

In Section 6, recent modifications made to the UA self-sustained combustion test facility are described.

In Section 7, PSIT modifications to EMAF to account for the degree of carbon burnout in modeling ash size and composition distributions during combustion under reducing stoichiometries are discussed. The results of a parametric study showing the effect of stoichiometric ratio on ash particle size and composition distributions obtained from combustion of washed Pittsburgh #8 coal is then presented. Differences in composition distributions are minor, reflecting primarily the increase in mineral coalescence associated with combustion under conditions of increasing stoichiometric ratio. Ash particle size distributions show an increase as stoichiometric ratio is increased.

In an Appendix to this report, analytical data generated and provided by Dr. Fraser Wigley of Imperial College are reproduced.

SECTION 2

OVERVIEW OF PROGRAM TASKS
(PSI Technologies)

2. OVERVIEW OF PROGRAM TASKS

This project is designed to examine the effects of combustion stoichiometry on the fundamental aspects of ash formation and ash deposit initiation. Emphasis will be placed on reducing stoichiometries associated with low-NOx combustion, although a range of oxidant/fuel ratios will be considered. Previous work has demonstrated that ash formation depends strongly upon coal mineralogy, including mineral type, size, amount, and the presence of organically associated inorganic species. Combustion temperature and the oxidation state of iron will also play a significant role. As these latter items will vary with changes in stoichiometry, research to determine the net effect on deposition is required.

To achieve these goals, a research program with the following technical objectives will be pursued:

(1) identify the partitioning of inorganic coal constituents among vapor, submicron fume, and fly ash products generated from the combustion of pulverized coal under a variety of combustion stoichiometries. Fuel-lean and fuel-rich combustion conditions will be considered.

(2) identify and quantify the fundamental processes by which the transformation of minerals and organically-associated inorganic species occur. Identify any differences from standard pulverized coal combustion conditions.

(3) modify, to incorporate the effects of combustion stoichiometry and based on the understanding developed in (1) and (2) above, an Engineering Model for Ash Formation. The previously developed model is capable of predicting the size and chemical composition distributions of the final ash products under standard pulverized coal combustion conditions of 20% excess air. These modifications will extend the model to include phenomena that may be dominant under a broad range of stoichiometries.

Experiments, sample analyses, and modeling will be conducted at several facilities as part of this program. Detailed coal and ash sample analysis using Mössbauer spectroscopy, x-ray absorption fine structure spectroscopy (XAFS), and computer controlled scanning electron microscopy will be carried out at the University of Kentucky (UKy). Small-scale drop tube combustion tests using size and density classified coal samples and possibly synthetic char samples will be carried out at the MIT to determine the extent of mineral coalescence and inorganic vaporization as a function of combustion stoichiometry. Combustion experiments utilizing utility grind coals will be conducted at PSI to examine the effects of stoichiometry on mineral interactions. Deposition experiments using ash generated from combustion experiments and using pure minerals will also be conducted to investigate deposit initiation as a function of combustion conditions. The engineering model for ash formation (EMAF) will be modified to include effects of combustion stoichiometry as part of this effort. Self-sustained pilot scale combustion experiments will be conducted in the University of Arizona (UA) 100,000 Btu/h

facility to address issues of scaling in combustion processes. The interaction of iron with aluminosilicates as a function of changing combustion conditions will be the focus of this effort. Modeling of the iron-aluminosilicate interaction process will be conducted as part of the UA study. Finally, interaction with an integrated program led by the utility PowerGen will be used to address issues of deposit formation at full scale for comparison with the bench and laboratory scale results of this program. A work breakdown structure containing a brief description of each task follows. The relationship among the participants is illustrated schematically in Figure 2-1.

Task 1 - Program Planning, Management, Reporting, and Peer Review

This task, to be performed by PSI Technologies, consists of: (1) preparing and annually updating a program plan; (2) coordinating, managing, and integrating the subcontracts and project results; (3) preparing project monthly reports; (4) integrating and preparing project quarterly reports; (5) integrating and preparing the program final report; (6) conducting annual peer review and project coordination meetings with the project principal investigators, either as a separate meeting or in conjunction with a technical conference, and including when appropriate the principal investigators of other DoE-supported ash formation research programs identified by the DoE project manager; and (8) acquiring and distributing coals to all of the project principal investigators.

Task 2 - Fundamental Study of Ash Formation and Deposit Initiation Under Reducing Conditions (PSI Technologies)

PSI will study the effect of combustion stoichiometry on mineral matter and inorganic species transformations with an emphasis on sub-stoichiometric combustion. This will occur through a series of experiments to be conducted in a well-characterized laboratory flow reactor on a minimum of two coals. Coal blends may also be examined if of benefit to the program and of mutual interest to PSI and DoE/PETC. One or more of the coals studied in this task may be coals previously studied at PSI under DoE contract number DE-AC22-86PC90751 to permit a direct comparison with results obtained under oxidizing conditions. Model mineral compounds will also be examined as necessary to identify the importance of the oxidation state of iron in determining mineral coalescence and ash deposition. Selection of any coal samples will be coordinated with the DoE/PETC program manager.

PSI will also conduct limited experiments to determine the effect of pyrite weathering on the evolution of an iron oxide fume. These experiments will be coordinated with a similar study at Sandia National Laboratories.

PSI will also conduct in-situ combustion experiments in conjunction with the University of Kentucky and Brookhaven National Laboratories using an in-situ combustion reactor at beamline X19-A of the National Synchrotron Light Source.

Activities under this task will include collection and examination of ash samples at varying combustion temperatures and/or oxidant concentrations. Ash samples will be collected using extractive sampling. In-situ deposit collection techniques will be used to measure ash

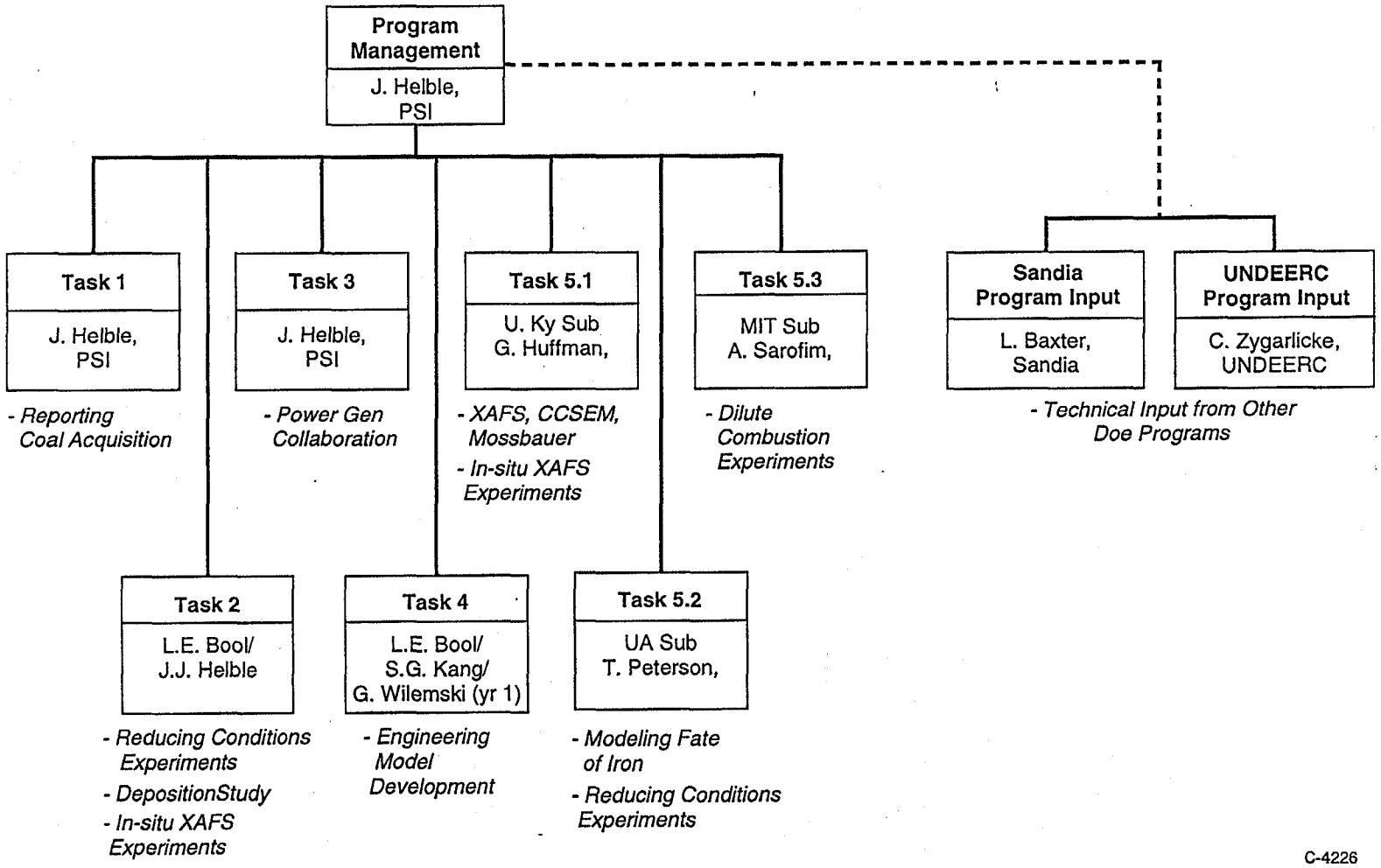

Figure 2-1. Program structure.

particle collection efficiencies as a function of temperature and stoichiometric ratio. Extracted ash and deposit samples will be characterized as necessary to determine particle size and chemical composition distributions as well as the chemical state of key components such as iron and calcium.

Task 3 - PowerGen Collaboration (PSI)

In order to understand the effects of combustion scale on ash formation and deposition under reducing conditions, PSI will interact with a government and industrial program currently underway in Great Britain. Led by the utility PowerGen, this program includes experiments at scales ranging from fundamental bench reactors to operating power plants. As part of a collaborative effort, PSI hopes to conduct laboratory experiments either at PSI, at BNL on the in-situ XAFS combustor, or in both reactors under a range of combustion conditions using a coal provided by PowerGen. If deemed appropriate by PSI, UA, and the DoE/PETC Program Manager, UA may also conduct combustion experiments with one of these coals. These experiments will permit direct comparison of results obtained in this project with those obtained at full scale in the PowerGen program. This interchange will also add to the database used in the modifications of the engineering model for ash formation described under Task 4.

Task 4 - Engineering Model for Ash Formation (PSI)

The results obtained by the organizations participating in this project will be applied by PSI to revise, test, and validate the EMAF developed previously. The work on this subtask includes analyzing the experimental results and identifying data and technical information related to extending EMAF. Specific areas of interest include the formation of ash under reducing stoichiometries, the formation (particularly the chemical composition) of the submicron ash fume, and the influence of char fragmentation on ash formation. As part of this task, PSI will also coordinate modeling activities to be conducted by the MIT and UA subcontractors.

Task 5.1 - Advanced Techniques for Coal and Ash Characterization Including In-situ XAFS Measurements (UKy)

The University of Kentucky will apply advanced analytical techniques such as computer-controlled scanning electron microscopy (CCSEM), Mössbauer spectroscopy, and x-ray absorption fine structure spectroscopy (XAFS) to characterize coal and ash samples from this program as needed by the individual principal investigators. If agreed upon by PSI, UKy, and the DoE program manager, UKy will also analyze selected coal and/or ash samples obtained from the PowerGen program in Great Britain.

As part of this task, UKy will conduct dynamic in-situ XAFS experiments at the Brookhaven National Laboratories (BNL) National Synchrotron Light Source (NSLS) with PSI and BNL using an in-situ drop tube furnace previously constructed by PSI. Static in-situ measurements at elevated temperatures will also be conducted using a cell previously built by UKy. The in-situ measurements will be used to investigate phenomena such as the transformation of pyrite under various conditions, the formation of iron aluminosilicate

compositions as a function of combustion conditions, the formation of calcium aluminosilicate ash compositions as a function of combustion conditions, and the composition and oxidation state of key components in sticky, depositing ash particles as a function of combustion conditions.

Task 5.2 - Pulverized Coal Combustion Studies Under Reducing Conditions in a Continuous, Self-sustained Laboratory Scale Reactor (UA)

UA will conduct experiments to assess the interaction of iron and aluminosilicate minerals under reducing combustion conditions. UA will also examine the amount and chemical composition of the submicron fume generated under reducing conditions. This study will be conducted in the UA self-sustained 100,000 Btu/h combustion facility. UA will conduct this study using at least one of the coals studied by PSI and MIT under this program and including at least one coal studied previously under oxidizing conditions. As part of the experimental effort, UA will conduct Auger analyses for samples provided by other principal investigators on an as-needed basis. UA will also conduct Mössbauer analysis on selected ash samples generated at UA.

Based upon the results generated in this program, UA will modify the previously developed model for iron aluminosilicate formation to incorporate additional coals and/or combustion conditions.

Task 5.3 - Fundamental Study of Mineral Interactions and Ash Vaporization Under Reducing Conditions (MIT)

MIT will conduct drop tube experiments to study the fundamental aspects of ash formation under sub-stoichiometric conditions using narrowly sized and density classified coal samples and/or synthetic char samples. Size segregated chemical composition measurements will be conducted to assess the release of inorganic species to the vapor phase under sub-stoichiometric conditions. MIT will also conduct fundamental coalescence experiments under reducing conditions to elucidate the mechanism and rate of interaction of key mineral pairs. MIT will assist in the EMAF model testing and validation as described under Task 4.

SECTION 3

TASK 2: COAL SELECTION AND CHARACTERIZATION
(PSI Technologies)

3. COAL SELECTION AND CHARACTERIZATION

CCSEM analyses of the washed Pittsburgh #8 coal and the Silverdale coal were also conducted by Dr. Fraser Wigley of Imperial College as part of a collaborative effort. The Silverdale sample examined by Dr. Wigley was part of a large combustion testing program being conducted in the U.K. and led by the utility PowerGen; the PSIT sample was obtained from National Power, also a participant in the U.K. program, and should be comparable to the sample examined by Dr. Wigley. The sample of washed Pittsburgh #8 examined by Dr. Wigley was a sub-sample split out of PSIT's sample and should therefore be nearly identical to the PSIT sample.

A comparison of Dr. Wigley's CCSEM analysis of the washed Pittsburgh #8 coal with that provided earlier by the University of Kentucky is shown in Figure 3-1. The distributions measured by UKy and Imperial College were nearly identical. Size distributions for the Silverdale coal, shown in Figure 3-2, differ in the smaller size bins as shown.

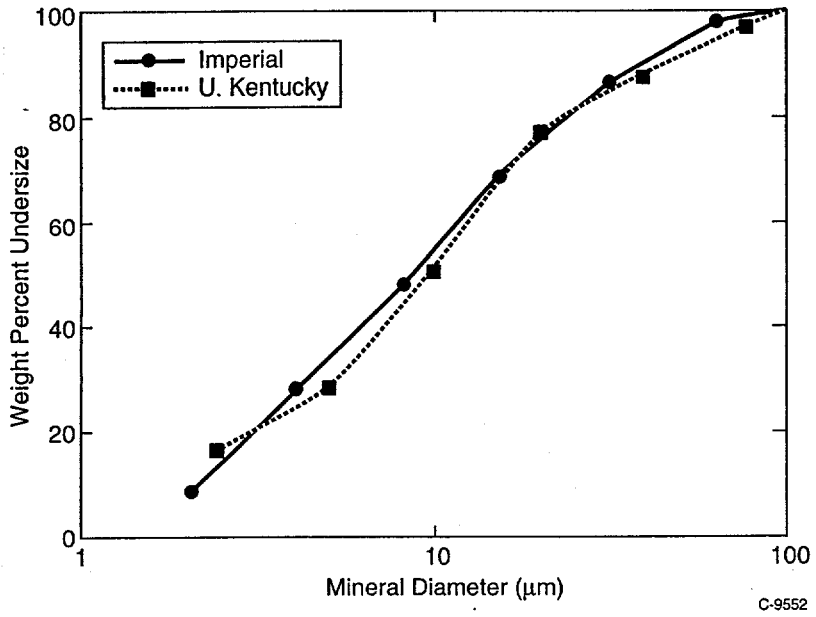

Figure 3-1. CCSEM mineral size distributions for the washed Pittsburgh #8 bituminous coal as measured by Imperial College and the University of Kentucky.

CCSEM mineral distributions for a third coal examined under this program, the Black Thunder sub-bituminous coal, have also been determined by another research group. Dr. John Harb of Brigham Young University is studying a sample of Black Thunder coal obtained from UND EERC in his program "Investigation of Mineral Transformations and Ash Deposition During Staged Combustion," program DE-FG22-93PC93226. The BYU sample of Black Thunder is believed to be similar to the one studied under this (PSIT) program. The mineral composition distribution reported by Dr. Harb in his Quarterly Technical Progress Report for the period January 1, 1994 to March 31, 1994 is compared with those obtained by University of

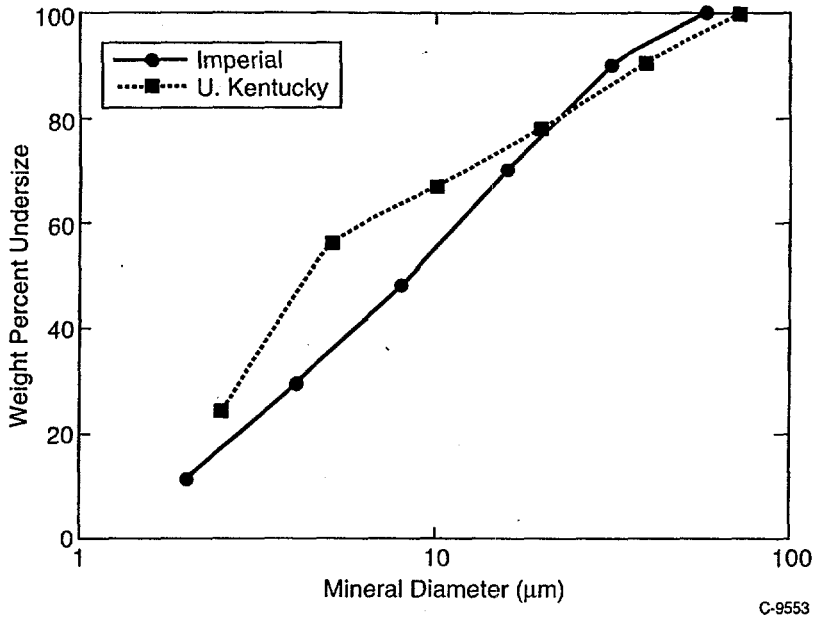

Figure 3-2. CCSEM mineral size distributions for the Silverdale bituminous coal as measured by Imperial College and the University of Kentucky.

Kentucky and UND EERC CCSEM analyses in Table 3-1. Mineral size distributions for the mineral quartz are compared in Figure 3-3. The BYU analysis was fairly close to the University of Kentucky analysis.

Table 3-1. Comparison of BYU-UND-UK Black Thunder Coal

	Weight % of Mineral Matter		
	UND, QR 3	UK, QR 3	BYU
Quartz	24.1	26.6	30
Iron Ox/Carb	4.6	0	6
Kaol/AlSi	29.1	38.2*	41
Montmorill	4.6	3.9	3
Pyrite	4.7	1.9	1
CaAl Phos	9.8	6.2	7
Other	16.0	23.2	18

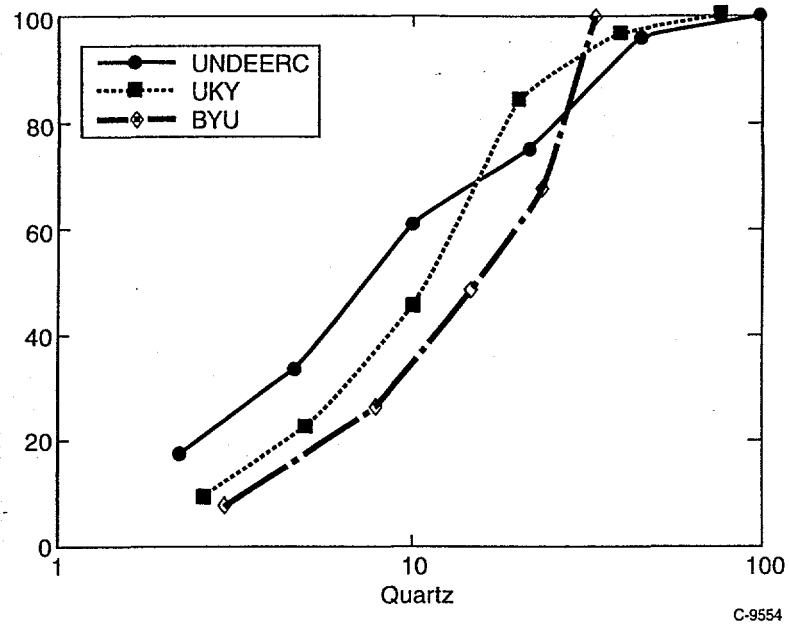

Figure 3-3. CCSEM quartz mineral distribution for the Black Thunder sub-bituminous coal as measured by UND EERC, Brigham Young University, and the University of Kentucky.

SECTION 4

TASK 5.1: ADVANCED TECHNIQUES FOR COAL AND ASH CHARACTERIZATION INCLUDING IN-SITU XAFS MEASUREMENTS

(University of Kentucky)

4. ADVANCED TECHNIQUES FOR COAL, MINERAL AND ASH CHARACTERIZATION

During the eighth quarter of this project, ash samples generated in laboratory experiments by PSIT, pilot scale combustion tests by DOE/PETC, and in full scale field trials by the utility PowerGen (as part of a complementary program being conducted in the U.K.) were analyzed by XAFS and Mössbauer spectroscopy. The results of these measurements are described below.

Ash Samples from Imperial College

Fly ash, bottom ash and probe deposit samples collected during field sampling at the PowerGen Ratcliffe (England) station in October 1992 were sent to PSIT by Imperial College for analysis. Ca K edge XANES data were collected on selected samples to investigate forms of Ca, and Mössbauer spectroscopy was used for the investigation of forms of Fe. These elements were selected because researchers at PowerGen and Imperial College have suggested that the chemical state of iron and calcium in the fly ash affects the deposition of ash during combustion of Silverdale coal. Similar conclusions have been reached by researchers in this program based upon extensive laboratory experimentation. Samples collected during the lowest oxygen partial pressure conditions (2.5 % excess oxygen as reported by Imperial College) were examined first. Mössbauer results for these samples are reported in Table 4-1. Data on the remaining samples are still being collected.

As seen in Table 4-1, there were significant differences between fly ash and bottom ash samples. In the bottom ash, the majority (78%) of iron was present in the α-Fe_2O_3 hematite phase, whereas the fly ash was enriched (57%) with magnetite. The total amount of iron present in glassy phases was higher in the fly ash sample. In both samples, the concentration of the (Fe^{+3}) iron in glass was similar but the concentration of the ferrous (Fe^{+2}) iron in glass is much lower in the bottom ash (2%) than the fly ash (15%). This difference translates to an order of magnitude difference in the Fe^{+2}/Fe^{+3} ratio, which would greatly affect the viscosity of the molten phase.

Probe deposit samples also show significant differences. Examining the bulk ash sample, the concentration of iron in glassy phases (82%) is considerably higher than that observed in either the fly ash or the bottom ash samples. The Fe^{+2}/glass concentration was eight times higher in the bulk deposit (72%) than the inner layer of the deposit (9%). The inner (initial) deposit also shows higher concentrations of α-Fe_2O_3 (31%) and magnetite (52%) phases. These results suggest that the iron may have crystallized out of the glass at the lower temperatures near the air-cooled probe surface, or that glassy phase iron does not contribute to iron-containing ash particle deposition. The latter conclusion is contrary to experimental and field data, so it is assumed that crystallization is a more likely explanation for the observed trend.

As shown in Figure 4-1, Fe K-edge XANES data were collected for selected fly ash and bottom ash samples. However, as discussed in the later parts of this report, currently we are unable to deconvolute the XANES spectra to quantify the contributions of various phases to the features of the spectra.

Table 4-1. Mössbauer spectroscopy results of samples collected during field sampling at the PowerGen Ratcliffe station. Silverdale coal was used during these tests.

CFFLS/ MK #	Sample	Phases	I.S.	Q.S.	Hfs	%Fe
95-030	510/F	Fe^{++}/Glass	0.86	2.26		15
2013	Fly ash	Fe^{+++}/Glass	0.44	0.83		18
	low pO_2	α-Fe_2O_3	0.38	-0.10	511	10
		Magnetite	0.33	0	484	25
		Magnetite	0.56	0	452	22
		Magnetite	0.58	0.04	410	10
95-033	573/S	Fe^{++}/Glass	0.85	1.64		2
2018	Bottom ash	Fe^{+++}/Glass	0.30	1.11		21
	low pO_2	α-Fe_2O_3	0.37	-0.11	504	45
		α-Fe_2O_3	0.37	-0.11	486	33
95-036	539/D	Fe^{++}/Glass	1.02	2.15		40
2010	Probe deposit,	Fe^{++}/Glass	0.90	1.54		32
	bulk, low pO_2	Fe^{+++}/Glass	0.49	-0.39		10
		Magnetite	0.17	0	480	7
		Magnetite	0.79	0	450	11
95-038	540/D	Fe^{++}/Glass	0.98	1.92		9
2011	Probe deposit,	Fe^{+++}/Glass	0.32	0.86		8
	inner, low pO_2	α-Fe_2O_3	0.35	-0.11	512	31
		Magnetite	0.27	0	485	23
		Magnetite	0.59	0	458	18
		Magnetite	0.62	-0.02	432	11

Figure 4-2 shows Ca-K edge XANES of some standard compounds. Wollastonite is a triclinic mineral form of $CaSiO_3$ and its spectra appears similar to that of a $CaSiO_3$ chemical compound (obtained from Alfa/Aesar chemicals). Stilbite is an aluminosilicate mineral of the zeolite family with a composition of $(Ca,Na)_3Al_5(Al,Si)Si_{14}O_{40}\bullet 15H_2O$. Figure 4-3 shows Ca-K edge XANES of the selected ash samples collected under high and low oxygen partial pressure conditions. XANES spectra features of all ash samples appear to show combinations of XANES spectral features of calcium silicate, calcium aluminosilicate and calcium sulfate. Samples collected under higher oxygen partial pressure show a better defined pre-edge peak and a more pronounced shoulder on the main peak indicating presence of higher amounts of calcium silicate. Unlike Fe (obtained by Mössbauer Spectroscopy) data, Ca K edge XANES spectra of bulk and inner deposits do not show any significant differences. We are currently experimenting with derivatives of these spectra in an attempt to bring out the structural differences between the samples more clearly.

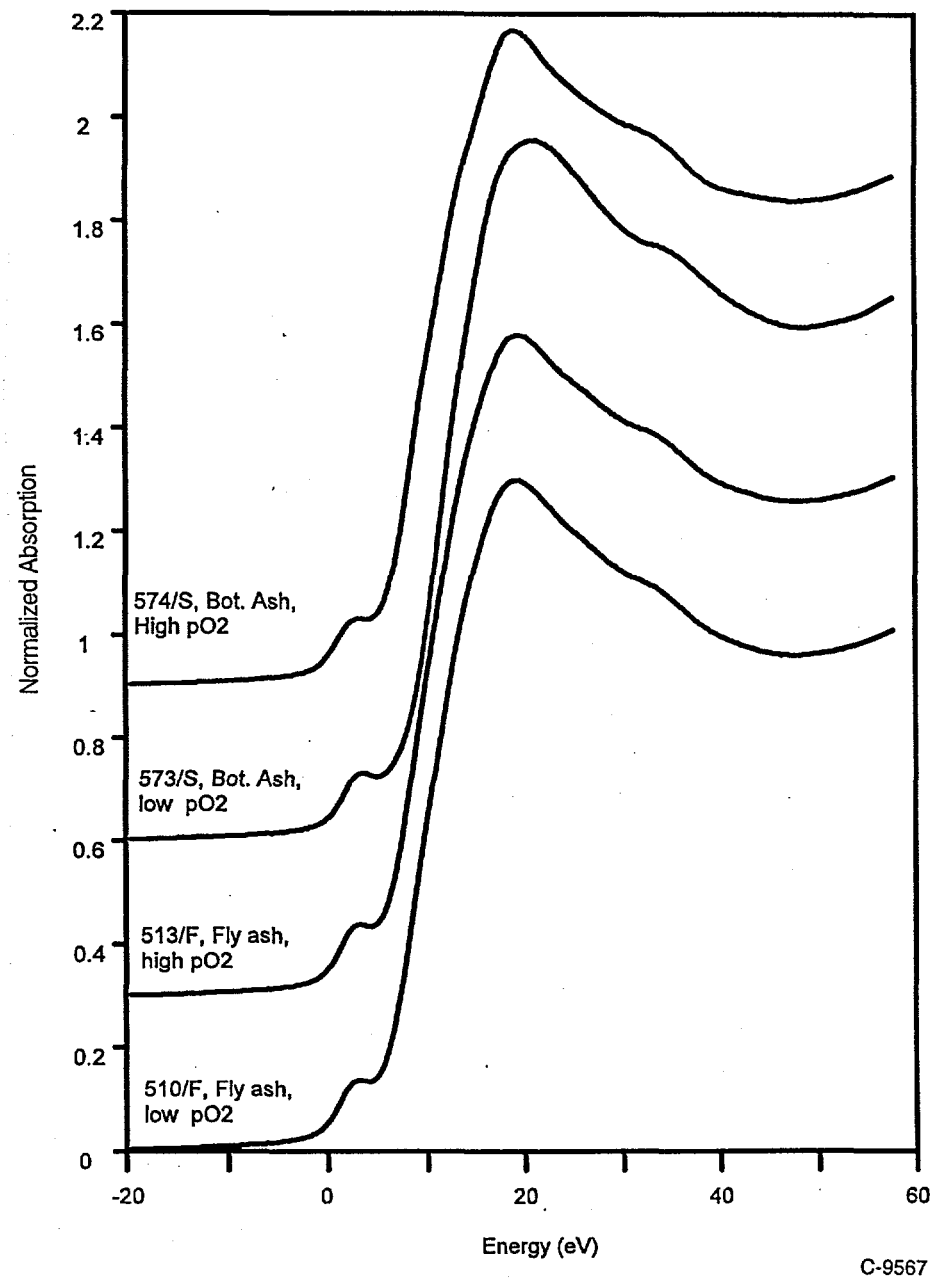

Figure 4-1. Fe K edge XANES of selected fly and bottom ash samples collected during PowerGen field test using Silverdale coal.

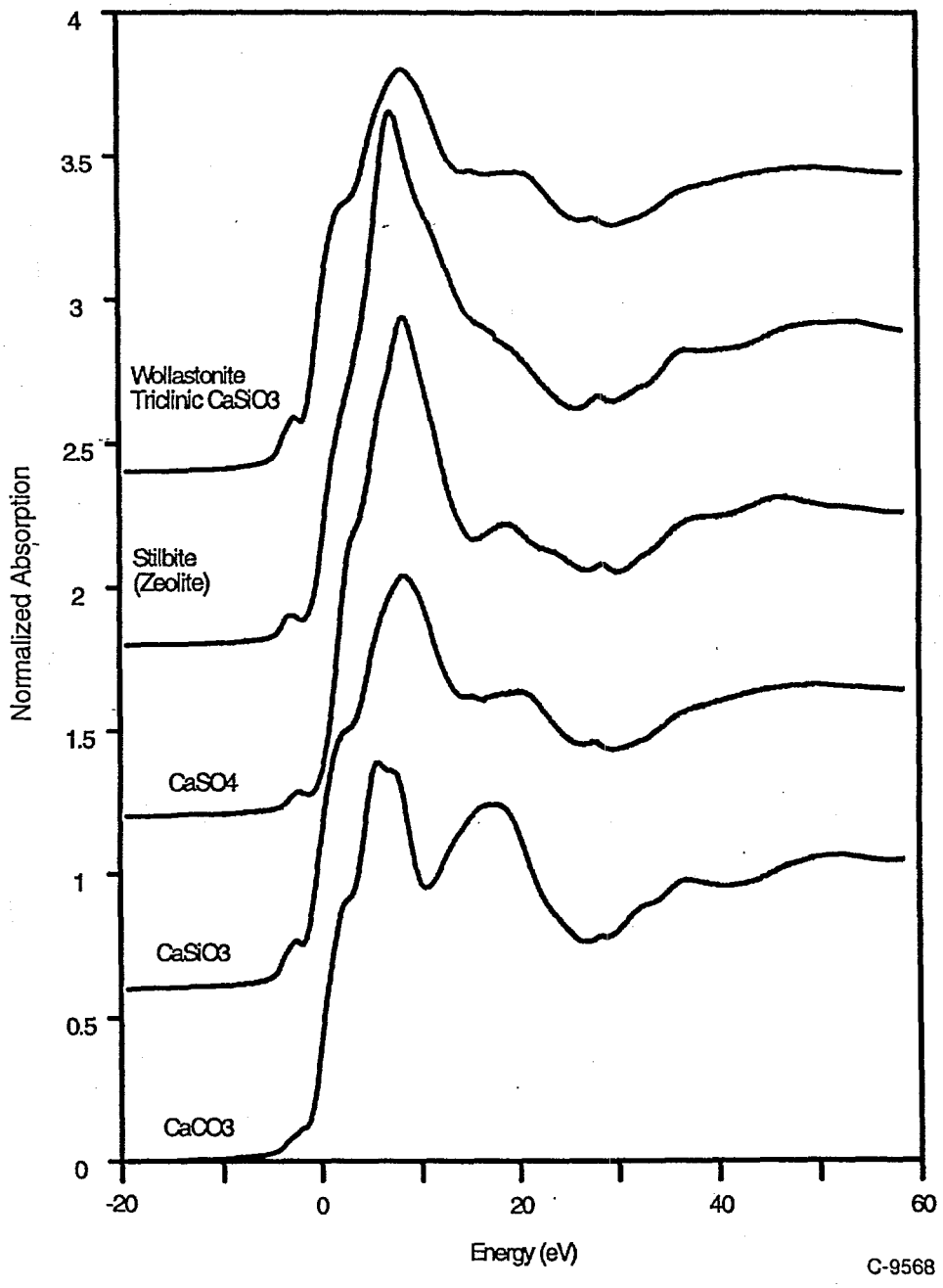

Figure 4-2. Ca K edge XANES of standard compounds and minerals.

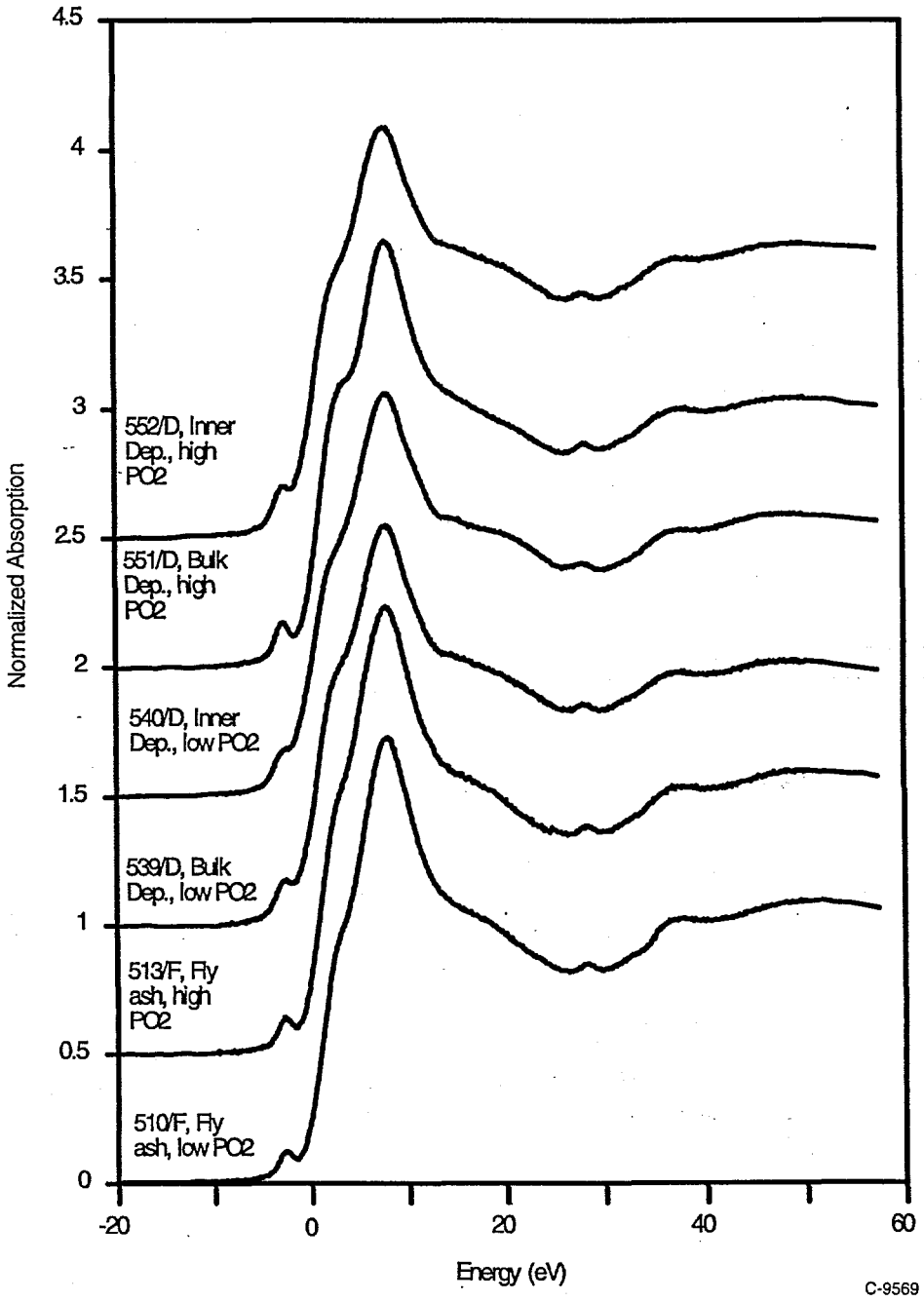

Figure 4-3. Ca K edge XANES of fly ash and deposit samples collected during field test at the PowerGen Ratcliffe Station burning Silverdale coal.

PSIT Laboratory deposit samples from combustion of Silverdale coal

To compare the ash formation and deposition behavior of the Silverdale coal in a power station field test with a laboratory drop tube furnace (with more controlled stoichiometric conditions), ash deposit samples were generated at PSIT. The PSIT experiments were conducted at a reactor temperature of 1773 K and a stoichiometric ratio of 1.2. Only one sample has been analyzed at this time (Table 4-2). The fraction of iron present in the glassy phase in the PSIT samples was approximately the same as that observed in the fly ash samples obtained in the Ratcliffe power station (Table 4-1).

Table 4-2. Mössbauer Spectroscopy results for PSIT lab deposit sample from combustion of Silverdale coal.

CFFLS / MK #	Sample	Phases	I.S.	Q.S.	Hfs	%Fe
95-040	4/25A	Fe^{++}/Glass	0.91	2.00		7
2015	PSIT	Fe^{+++}/Glass	0.30	1.14		19
	deposit	Magnetite	0.30	0	487	32
	SR=1.2	Magnetite	0.67	0	454	25
		Magnetite	0.38	-0.08	362	17

Figure 4-4 shows Ca K edge XANES of the three PSIT drop tube furnace Silverdale deposit samples. Once again it appears that the combustion conditions have negligible effect on the distribution of the forms of calcium in the deposit. The pre-edge peak and the shoulder on the low energy side of the main peak are more pronounced in PSIT deposits than in the PowerGen field test which would suggest that the partial pressure of oxygen in the PSIT tests is higher. However, unlike the PowerGen field test, these features do not change with different stoichiometric ratios.

PETC pilot scale combustor generated fly ash samples of washed Pittsburgh #8 coal

A washed Pittsburgh #8 coal, similar to the washed Pittsburgh #8 examined in this program, was burned in the DOE/PETC fuels evaluation furnace. Fly ash samples collected from this burn were analyzed by Mössbauer spectroscopy. Results for the DOE washed Pittsburgh #8 coal and fly ash samples from combustion in the PETC combustor using low NO_x burner conditions are reported in Table 4-3. Analysis of the PSIT washed Pittsburgh #8 coal examined in this program is also shown in Table 4-3; pyrite levels were similar to those measured in the PETC sample. In the PETC combustion measurements, it appears that the transformations of the iron phases is complete at 1.7 sec residence time, as there are no further changes in the distribution of the forms of Fe at longer times.

This coal was also combusted at PSIT and MIT under varying residence time and stoichiometric conditions. Mossbauer results of the ashes generated from those experiments

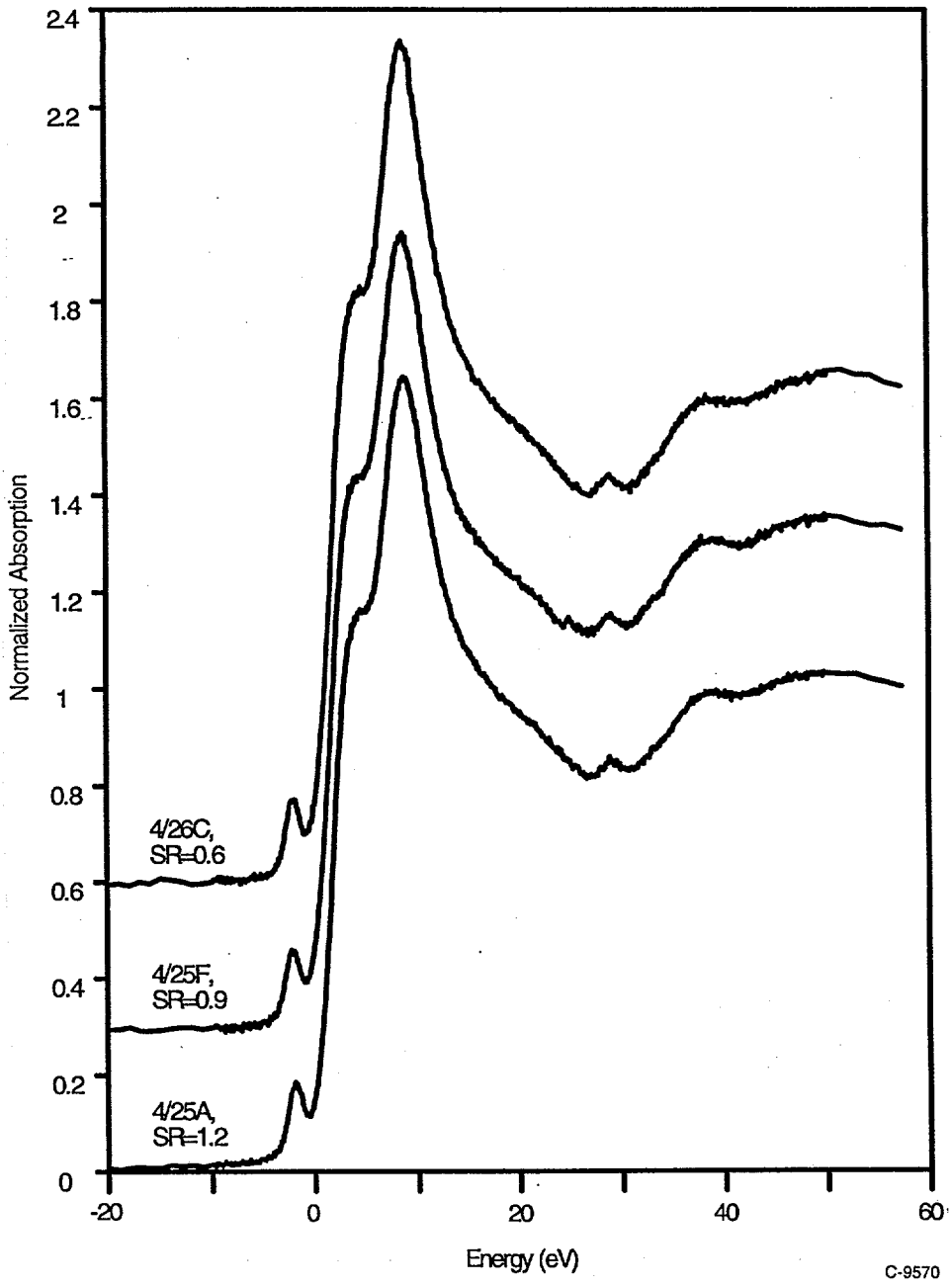

Figure 4-4. Ca K edge XANES of PSIT drop tube furnace deposit samples generated using Silverdale coal.

have been reported in Quarterly Report number 4 (for the period 1/1/94 to 3/31/94). The amount and distribution of iron in glassy phases in the PETC samples is closest to the amounts and distribution observed for the oxygen rich short residence time samples generated at PSIT.

Table 4-3. Mössbauer Spectroscopy results for DOE washed Pittsburgh #8 coal and fly ash samples from combustion in the PETC pilot scale combustor, low NO_x burner conditions.

CFFLS / MK #	Sample	Phases	I.S.	Q.S.	Hfs	%Fe
MK 1698	washed Pitt #8 coal (PSIT)	Pyrite Illite (clay) Siderite				90 7 3
95-043 2009	Washed Pitt #8 coal	Pyrite Illite (Clay) Jarosite	0.30 1.23 0.38	0.61 2.74 1.04		88 6 6
95-044 2008	#25, ash 0.9 sec	Fe^{++}/Glass Fe^{+++}/Glass Magnetite Magnetite Magnetite	0.83 0.56 0.28 0.67 0.37	1.94 0.71 0 0 -0.09	 490 458 515	20 11 25 37 7
95-045 2005	#26, ash 1.7 sec	Fe^{++}/Glass Fe^{+++}/Glass α-Fe_2O_3 Magnetite Magnetite	0.77 0.37 0.37 0.64 0.29	2.36 0.96 -0.09 0 0	 515 456 491	5 22 27 20 26
95-046 2006	#27, ash 2.6 sec	Fe^{++}/Glass Fe^{+++}/Glass α-Fe_2O_3 Magnetite Magnetite	0.90 0.28 0.36 0.27 0.62	1.71 1.16 -0.08 0 0	 514 489 457	2 19 31 22 26

Samples generated during combustion at stoichiometric ratios ranging from 0.6 to 1.2 had higher percentages of iron in the glassy phase iron and lower Fe^{+3}/Fe^{+2} ratios than the PETC samples.

In situ XAFS combustor test

In February of 1995 under separate DOE support, Dr. Shin Kang and Dr. Larry Bool of PSIT carried out maintenance of the *in situ* XAFS combustor at Brookhaven National Laboratory. At that time they also ran the combustor under different combustion condition and collected ash samples from the combustion of washed Pittsburgh #8 coal. Subsequently, this coal was combusted at PSIT under same conditions and the samples were collected to compare

with whose collected from *in situ* combustor. We have now carried out Mössbauer and static Fe XAFS experiments and the results are discussed here (Table 4-4).

Table 4-4. Mössbauer Spectroscopy of ashes from combustion of DOE washed Pittsburgh #8 coal. Samples 1 to 5 were obtained with BNL *in situ* XAFS combustor and samples 6 to 12 were obtained with PSIT combustor

CFFLS / MK #	Sample	Phases	I.S.	Q.S.	Hfs	%Fe
95-091 2067	#1, BNL 1200 °C, SR=1.2, %C=41	Fe^{++}/Glass Fe^{+++}/Glass α-Fe_2O_3 Magnetite Magnetite	0.97 0.34 0.36 0.28 0.65	1.92 0.77 -0.09 -0.01 -0.02	 515 490 458	3 4 56 20 17
95-092 2068	#2, BNL 1200 °C, SR=2, %C=21	Fe^{+++}/Glass α-Fe_2O_3 Magnetite Magnetite	0.34 0.36 0.33 0.53	0.95 -0.20 -0.07 -0.02	 515 492 453	9 78 8 5
95-093 2069	#3, BNL 1200 °C, SR=10, %C=24	Fe^{+++}/Glass α-Fe_2O_3 Magnetite Magnetite	0.30 0.36 0.59 0.34	0.96 -0.09 0.03 -0.07	 516 456 492	7 74 8 11
95-094 2070	#4, BNL 1400 °C, SR=10, %C=25	Fe^{+++}/Glass α-Fe_2O_3 Magnetite Magnetite	0.33 0.36 0.29 0.66	0.96 -0.10 -0.04 -0.01	 515 490 457	10 61 14 15
95-095 2071	#5, BNL 1400 °C, SR=1.2, %C=74	Fe^{++}/Glass Fe^{+++}/Glass α-Fe_2O_3 Magnetite Magnetite	1.13 0.32 0.36 0.66 0.25	2.00 0.88 -0.08 0 0	 514 456 487	16 14 31 23 16
95-049 2041	#6, PSIT 1200°C, SR=10,%C=2	Fe^{+++}/Glass α-Fe_2O_3 α-Fe_2O_3	0.30 0.36 0.30	0.91 -0.11 -0.08	 515 477	17 64 19

CFFLS / MK #	Sample	Phases	I.S.	Q.S.	Hfs	%Fe
95-048	#7, PSIT	Fe^{+++}/Glass	0.31	0.99		18
2042	1200°C,	α-Fe_2O_3	0.37	-0.11	512	48
	SR=2, %C=4	Magnetite	0.33	-0.06	490	20
		Magnetite	0.56	-0.04	452	14
95-047	#8, PSIT	Fe^{++}/Glass	0.98	1.34		33
2043	1200°C,	Fe^{+++}/Glass	0.22	0.49		6
	SR=1.2, %C=60	α-Fe_2O_3	0.39	-0.12	515	8
		Magnetite	0.26	0	489	20
		Magnetite	0.67	0	456	33
95-050	#9, PSIT	Fe^{+++}/Glass	0.32	1.16		19
2048	1400 °C,	α-Fe_2O_3	0.37	-0.10	515	59
	SR=10, %C=2	α-Fe_2O_3	0.37	-0.08	494	22
	#10, PSIT	Fe^{++}/Glass	0.68	2.33		6
95-052	1400 °C,	Fe^{+++}/Glass	0.39	0.97		21
2044	SR=2, %C=3	Magnetite	0.31	0	490	40
		Magnetite	0.62	0	454	33
95-051	#11, PSIT	Fe^{++}/Glass	0.80	0.79		29
2046	1400 °C,	Fe^{++}/Glass	1.03	1.92		26
	SR=1.2, %C=39	Magnetite	0.27	0	488	13
		Magnetite	0.67	0	456	29
		Magnetite	0.77	0	307	3
95-053	#12, PSIT	Fe^{++}/Glass	0.71	2.34		6
2047	1400 °C,	Fe^{+++}/Glass	0.39	0.92		17
	SR=2, %C=17	α-Fe_2O_3	0.37	-0.08	514	15
	unquenched	Magnetite	0.30	0	492	33
	total filter	Magnetite	0.61	0	454	29

Examination of the Mössbauer spectroscopy data reveals some differences between the two samples in the iron phase distribution. All samples generated at PSIT demonstrated higher fractions of iron in the glassy phases than did samples generated under identical conditions at Brookhaven, despite PSIT samples generally having *lower* concentrations of carbon. For all samples, the Fe^{+3}/Fe^{+2} phase distribution was similar between the facilities with the exception of the lowest temperature, lowest S.R. runs. PSIT data for this 1200°C, SR=1.2 run are consistent with data obtained at other conditions, whereas the amount of iron in glassy phases measured in the Brookhaven sample generated under the same conditions is unexpectedly low. The consistently higher percentage of glassy phase iron observed in the PSIT samples indicates that

there has been much greater reaction between pyrite and clay-derived phases in the PSI drop tube furnace. However, both furnaces show similar trends of increasing amounts of ferrous iron in glass and the magnetite/hematite ratios with decreasing stoichiometric ratios.

Figures 4-5 and 4-6 compare Fe K edge XANES data for ash samples produced in PSI and BNL tests at furnace set points of 1400 and 1200°C respectively. XANES and EXAFS data do not show any dramatic changes with changing combustion conditions. However, when we take third derivative of the XANES, then systematic changes are observed. Third derivatives of the XANES of samples exhibiting similar composition (as measured by Mössbauer spectroscopy) are similar. We are developing methodology to deconvolute the features of third derivatives of XANES and assign them to the individual forms of Fe present.

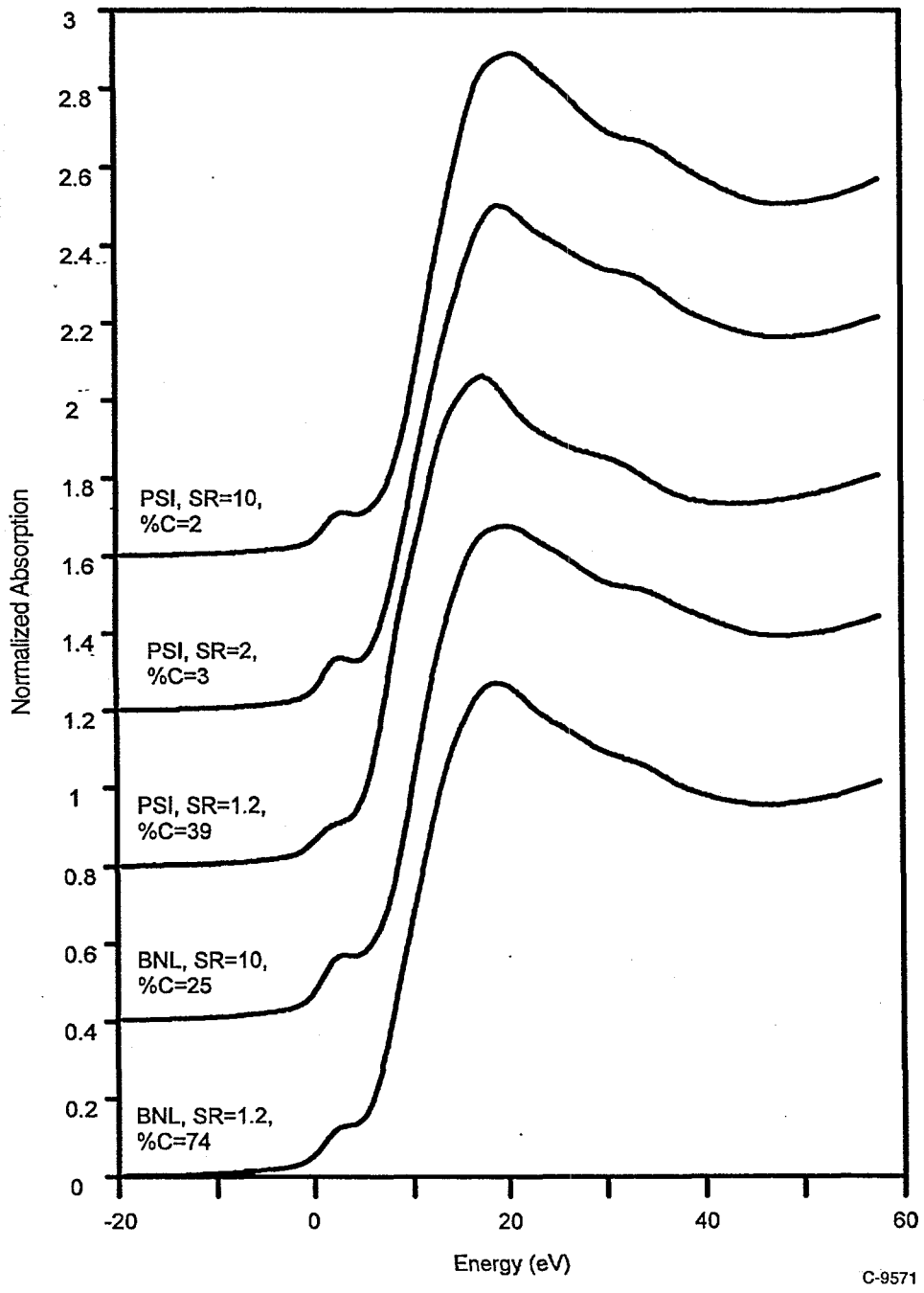

Figure 4-5. Fe K edge XANES of PSI and BNL drop tube furnace generated ash samples for washed Pittsburgh #8 coal. Furnace temperature set point = 1400 C.

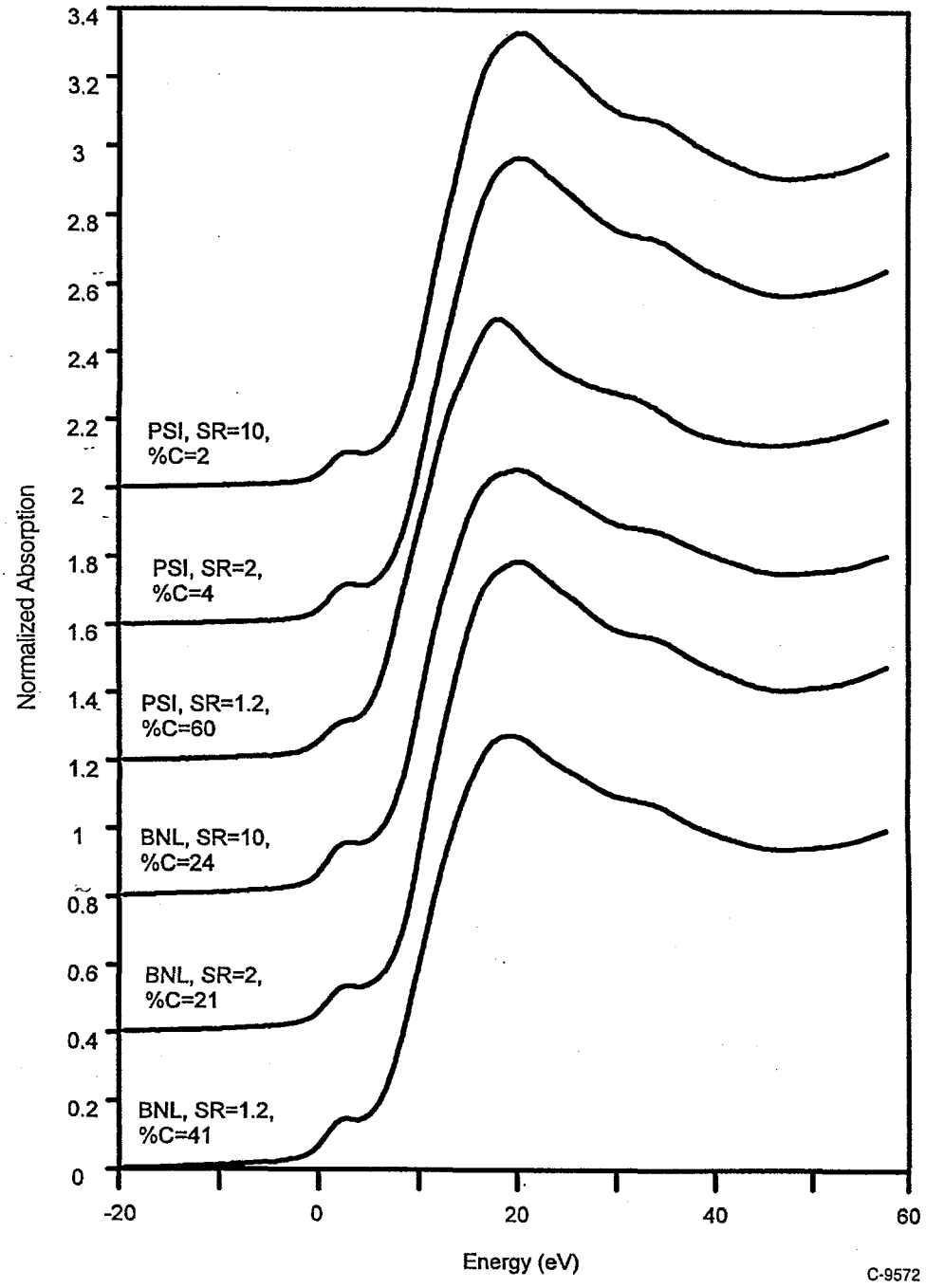

Figure 4-6. Fe K edge XANES of PSI and BNL drop tube furnace generated ash samples for washed Pittsburgh #8 coal. Furnace temperature set point = 1200 C.

SECTION 5

TASK 5.3: **FUNDAMENTAL COMBUSTION STUDIES UNDER REDUCING CONDITIONS**

(Massachusetts Institute of Technology)

5. FUNDAMENTAL COMBUSTION STUDIES UNDER REDUCING CONDITION

In the previous report, calculations were made to obtain the concentrations of CO, CO_2 and O_2 surrounding the burning char particle, and the combustion temperature of the particle. As part of the broader modeling effort, the vaporization rates of iron during the coal combustion during the past quarter.

5.1 Reducing Mechanism

It is generally believed that refractory oxides such as SiO_2, CaO, et al. are much more difficult to be vaporized than the corresponding volatile suboxide or metal. As shown in the previous report, CO dominates for the environment on the particle surface. For iron, one possible mechanism for vaporization is:

$$FeS + CO \leftrightarrow COS + Fe\ (gas)$$

as discussed by Graham (1991). Other mechanisms are also being evaluated. This reaction is assumed to be at equilibrium at the surface of each inclusion within the char particle. And the partial pressure of Fe at the inclusion surface is determined from the equilibrium constant Ke and the local gas compositions:

$$Ke = \frac{P\ ^{e}Pcos}{aPco}$$

where a is the activity of FeS, which is equal to 1. Since there is no other source of COS, the concentration of COS is taken to be of the same concentration as Fe. Therefore the concentration of Fe can be calculated by the following equation:

$$P = Pcos = (\ Ke\ Pco\ )^{1/2}$$

5.2 Calculation Strategy

The methods to calculate the vaporization rates of Fe is based upon the work by Quann (1). However, as we include a more rigorous estimation of the concentrations of CO, CO_2 and O_2, and the particle sizes during the combustion, calculations therefore include few assumptions than that by the previous researchers. For example, Quann assumed that

$$r_p = r_0\ (\ 1 - t/t_b\ )^{1/2}$$

which is valid in the diffusion controlled limit.

5.3 Calculation Results

As shown in the figures, we have estimated how that the partial pressure of Fe on the particle surfaces and the vaporization rates change with time (particle size). By integrating the rates, we can obtain the total Fe vaporized. This result is in good agreement with the experimental data.

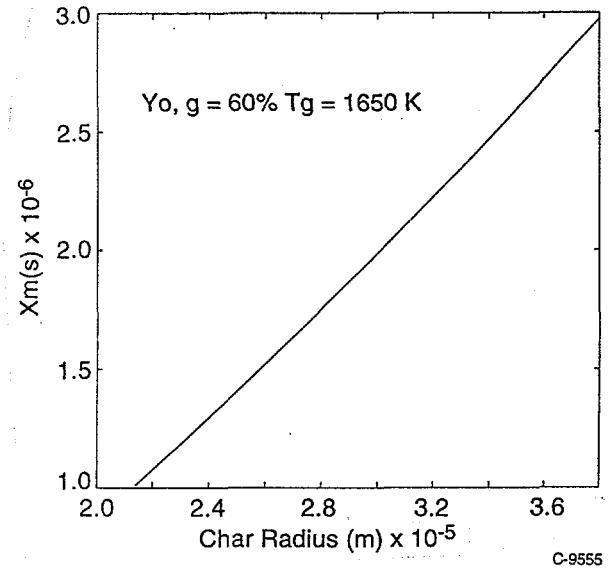

Figure 5-1. Fe vapor mole fraction at char surface as a function of particle size.

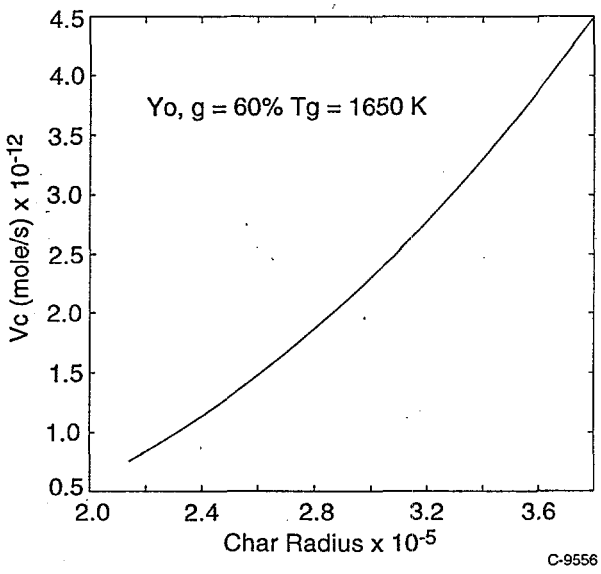

Figure 5-2. Fe vaporization rate as a function of particle size.

References

Graham, K.A., Ph.D. Thesis, M.I.T. Department of Chemical Engineering, Cambridge, MA (1991).

Quann, R. J. and Sarofim, A.F., Vaporization of Refractory Oxides During Pulverized Coal Combustion, Nineteenth Symposium (international) on Combustion / The Combustion Institute, 1982 , pp. 1429-1440

SECTION 6

TASK 5.2: **LARGE SCALE COMBUSTION STUDIES**
(University of Arizona)

6. LARGE SCALE COMBUSTION STUDIES

Large Furnace

Work continued rebuilding parts of the large furnace. The main work concentrated on the rebuilding of the burner. A schematic of the burner is shown in Figure 6-1. The burner consists of two concentric 316 stainless steel pipes. The outer pipe has an outer diameter of 4.5 in., an inner diameter of 4.3 in., and is used as a cooling water jacket. The inner pipe has an outer diameter of 2.375 in. and an inner diameter of 2.067 in. The inner tube is the coal feed to the furnace. Coal is fed to the inner tube from the coal screw feeder through an 1/2 in. tube.

In order to prevent heating the coal prior to entering the furnace and possible flashback in the natural gas line, a cooling water mesh was added to the inner tube. The mesh consisted 12 of 1/8 in. 316 stainless steel tubes, six in each direction across the inner tube. See Figure 6-2. The cooling water mesh tubes come from a common header and are open to the cooling water jacket at the other end. The cooling water is added from the top of the burner and is removed at the top of the cooling water jacket. Both the inlet and outlet use 3/8 in. stainless steel tubes. The cooling water inlet is inside of the water jacket to provide additional cooling to the inlet tube and to ease the manufacturing of the burner. The cooling water outlet is equiped with a thermocouple to monitor its temperature.

The furnace is heated using natural gas until it is self-sustaining. The natural gas is added using 1/4 in." stainless steel tubing. See Figure 3. The natural gas enters at a 5° pitch and the tubes are off center to provide clockwise rotation of the gas. This increases the turbulent mixing of the gas. The gas inlets are located one inch below the cooling water mesh. To ease the building of the burner, the natural gas line is also inside of the cooling jacket. This cools the natural gas prior to entering the furnace, so some of the heating value of the gas is lost.

Primary air is added to the furnace using a 1/2 in. tube. The primary air inlet is pitched at a 5° angle and is constructed to cause counter-clockwise rotation of the air. This should help to prevent the coal from adhering to the walls of the burner. The air inlet is right below the coal feed, so that the coal is mixed with the primary air as soon as possible.

As an additional safety feature, a thermocouple is added to the burner to monitor the temperature inside of the burner. The thermocouple is located in the center of the inner tube and halfway down the length of the tube. This will give adequate indication if the coal is being heated prematurely.

Due to problems with obtaining the stainless steel parts, the manufacturing of the burner took much longer than anticipated.

Drop Tube Furnace

Experiments continued with the drop tube furnace. Runs using the Pittsburgh #8 have been started. However, there is no data at this time. There has been some trouble with the

Mossbauer equipment with the calibration and the wave form. It is believed that these problems have been fixed and samples have been submitted to analyze. Samples have also been submitted to an analytical lab to determine the carbon content of the samples, in order to determine the amount of burnout that is occurring within the drop tube furnace.

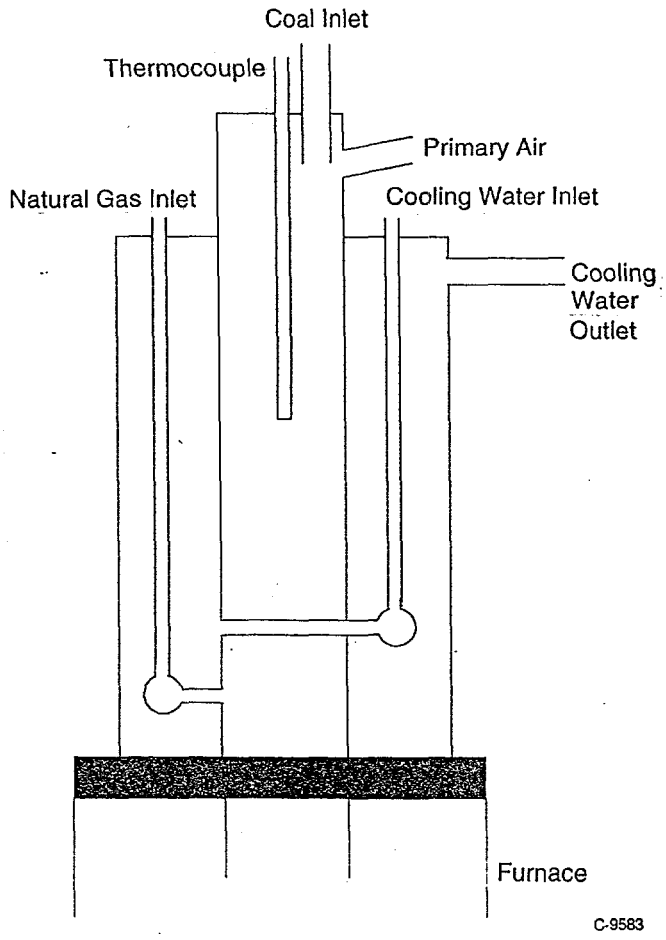

Figure 6-1. Schematic of Burner, Outside View

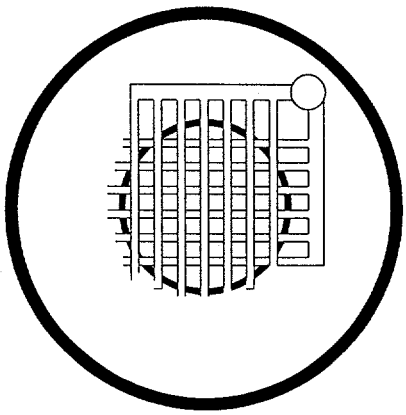

Figure 6-2. Cooling Water Mesh, Top View

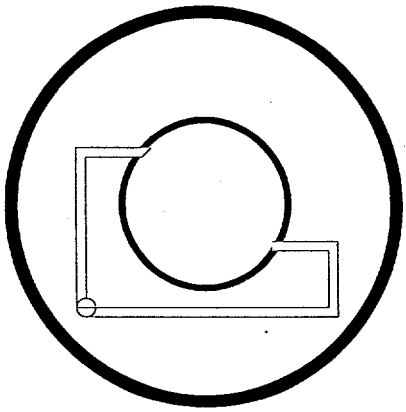

Figure 6-3. Location of Natural Gas Ports, Top View

SECTION 7

TASK 4: **ENGINEERING MODEL FOR ASH FORMATION**

(PSI Technologies)

7. ENGINEERING MODEL FOR ASH FORMATION

One of the major goals in this program is to modify the Engineering Model for Ash Formation (EMAF) to incorporate ash formation behavior that is unique to reducing environments. Previous experimental work in this program at PSIT and MIT has shown that the degree of carbon burnout plays a major role in mineral matter transformations during combustion under reducing environments and in deposition characteristics (e.g. stickiness) of the resulting ash. Therefore in order to use EMAF to model the ash size distribution and composition distributions for combustion under reducing conditions it was necessary to modify the model to account for the presence of unburned char. This modification was accomplished by developing a kinetic submodel, based on information in the literature, to predict the fraction of unburned char in each particle size range.

The kinetic submodel used here is similar to that discussed elsewhere (Bool et al., 1995, Helble et al 1992). In this submodel, the fractional burnout of char in a given size range is calculated by simultaneously solving for the burnout of all the size ranges present in the coal. For example, a coal with a particle size distribution ranging from 10 μm to 120 μm is divided into 12 size bins. The kinetic submodel then simultaneously solves the 12 rate equations describing burnout in the individual size bins. By simultaneously solving for the oxygen, carbon monoxide, and carbon dioxide concentrations, the submodel predicts which particles burn out first, and as a result predicts the degree of burnout for all size ranges.

The char burnout relation used, Eq. 1, was taken from Hurt and Mitchell (1992). According to this empirical study, the global char burnout rate is a function of the char external

$$\frac{d(CHAR)}{dt} = -K_c \exp\left(\frac{-E_c}{RT_p}\right) SA_{char} (P_{O_{2s}})^{1/2} \qquad (1)$$

surface area (SA_{char}) and the char particle temperature (T_p). To simplify the kinetic submodel, the char burnout temperature is set equal to the gas temperature - a reasonable assumption for sub-stoichiometric combustion. The gas temperature profile used in these calculations was that presented in Quarterly Report Number 3. The burnout rate was assumed to be proportional to the square root of the surface oxygen partial pressure (Po_{2s}). Finally, the global rate constants were determined empirically (by fitting to data from several coals) to be a function of the coal carbon content (%C, ash and H_2O free) as shown in Eqs. 2 and 3 (Hurt et al, 1992), where T_{ref} here is equal to K.

$$E_c = -5.945 + 0.355(\%C) \qquad (2)$$

$$\ln K_c = (2.80 + 0.0758(\%C)) - \left(\frac{E_c}{T_{ref} R}\right) \qquad (3)$$

It should be noted that Hurt et al. (1992) found that the lower rank coals burned in the diffusion limited regime. This fact was taken into account during the derivation of the parameters in Eqs. (2) and (3). Therefore, the model allows lower rank coals to burn much faster than the bituminous coals.

In the kinetic submodel the combustion product is assumed to be CO. The CO is then oxidized to CO_2 in the bulk gas phase according to Eq. (4). The global forward and

$$CO + 1/2\ O_2 \rightleftharpoons CO_2 \tag{4}$$

reverse reaction rates, R_f and R_b, shown in Eqs. (5) and (6), are those presented by Dryer et al (1973) and Westbrook et al (1981) respectively. The species concentrations are determined

$$R_f = 3.8x10^{14}\ V_g \exp\left(\frac{-E_{CO}}{R\ T_g}\right)\ [CO]\ [H_2O]^{1/4}\ [O_2]^{1/2} \tag{5}$$

$$R_b = 1x10^{11}\ V_g \exp\left(\frac{-E_{CO}}{R\ T_g}\right)\ [CO_2] \tag{6}$$

from the number of moles of each species in the system and the gas volume (from Eq. (7)). Mole balances for O_2, CO, CO_2 are shown in Eqs. (8) through (10). Finally, the surface partial pressure of oxygen is determined by assuming a steady state between oxygen transport and consumption (see Equation (11)).

$$V_g = \frac{n_t\ R\ T_g}{p} \tag{7}$$

$$\frac{d\{O_2\}}{dt} = \frac{1}{24}\left(\Sigma\frac{d(CHAR)}{dt}\right) + \frac{1}{2}(R_b - R_f) \tag{8}$$

$$\frac{d\{CO\}}{dt} = -\frac{1}{12}\left(\Sigma\frac{d(CHAR)}{dt}\right) + (R_b - R_f) \tag{9}$$

$$\frac{d\{CO_2\}}{dt} = R_f - R_b \tag{10}$$

$$\left(\frac{D}{r_c}\right)\left(\frac{P_{O_2}-P_{O_{2s}}}{R\ T_g}\right) = \frac{-k_c}{24}\exp\left(\frac{-E_c}{R\ T_p}\right)(P_{O_{2s}})^{1/2} \tag{11}$$

Because there is no simple means to take into account the coal devolatilization, we assumed (in EMAF) that devolatilization has taken place before the char begins to burn. The initial amounts of each of the gaseous species are determined from the coal mass, the stoichiometric ratio, and the fraction of volatile matter.

A typical burnout distribution is shown in Figure 6-1 for the washed Pittsburgh No. 8 examined in this program. This plot shows that as the stoichiometric ratio is increased, the small particles burn out before the larger particles. This result is reasonable given that during the shorter residence time required to completely burn the small particles, the particles experience oxygen rich conditions. However, as these small particles burn the oxygen is largely consumed - resulting in fuel rich conditions. The burnout of the larger particles is therefore prolonged because they combust primarily under fuel rich conditions. Figure 6-2 shows a comparison between the fraction carbon in the ash predicted by the kinetic submodel and that measured as part of the experimental procedure. The data shown here are for the three Pittsburgh No. 8 program coals (i.e. run-of-mine, washed, and beneficiated). There is reasonable agreement between the data and the predictions, but further comparisons with a wider range of coals and conditions are required to fully validate the submodel.

The output of this kinetic submodel is then used in EMAF to define the fraction of minerals in each simulated coal particle that is **not** exposed to the outer char particle surface during the combustion process. These minerals will generally maintain the same size and composition, since they cannot interact with other minerals. The remaining minerals are assumed to coalesce and interact with other minerals; this is the approach taken in the original version of EMAF for super-stoichiometric combustion conditions. Based on these mechanisms, the model predicts the size and composition distributions of the ash. Figures 6-3 and 6-4 illustrate the predicted changes in ash size and composition as a function of stoichiometric ratio for the run-of-mine Pittsburgh No. 8. On one extreme is the 1 ash per mineral case, which would match those conditions where very little char burnout has taken place, such as low residence times or stoichiometric ratios. The other extreme is the completely burned out case (SR=1.2). The model predicts a smooth transition of ash mass to the larger sizes with increasing stoichiometric ratio - indicating an increase in ash coalescence with stoichiometric ratio. This increase in coalescence is also evident in the composition predictions (Figure 6-2). The minerals are initially (on an oxygen, carbon, and hydrogen free basis): Si Al K, Si, Si Al, and lesser amounts of Si Al Fe and Si Al Ca. As these minerals coalesce, the amounts of Si (quartz) and Si Al K (illite) decrease, while the amount of Si Al increases. This is due to the fact that the

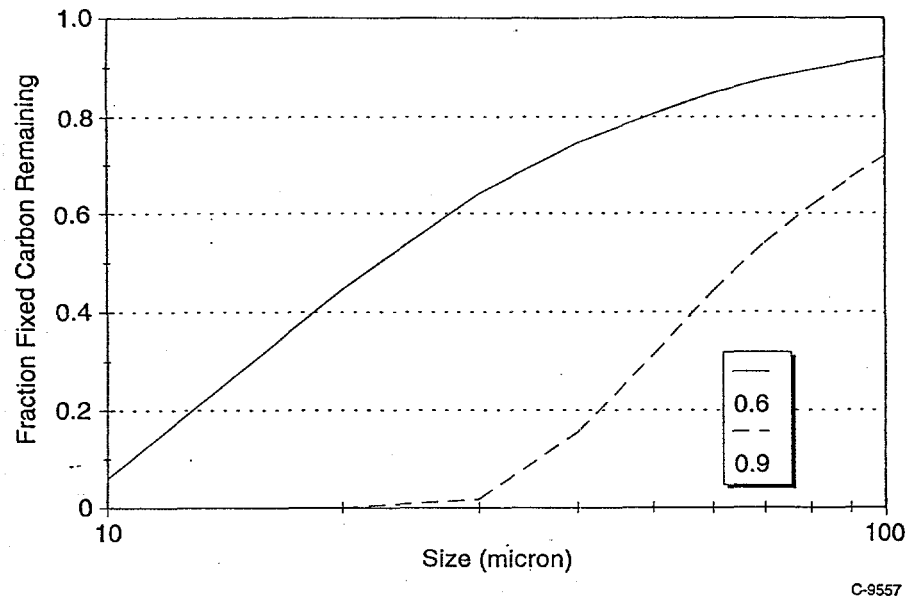

Figure 7-1. Fractional burnout by size - DOE Pittsburgh No. 8.

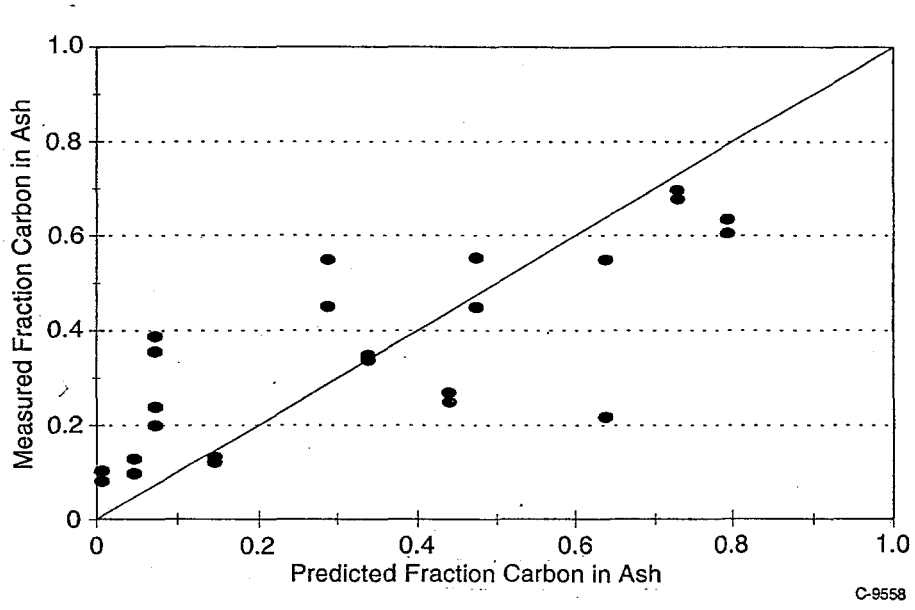

Figure 7-2. Burnout predictions for program coals - carbon content from deposition samples.

product of Si and Si Al K mixing has a lower K content and is binned (by EMAF) in the Si Al category. There is also evidence of increased Fe - silicate coalescence as a function of stoichiometric ratio (burnout), which is qualitatively consistent with the experimental data for this coal. Additional model modifications and validation will be accomplished during the final quarter of this program.

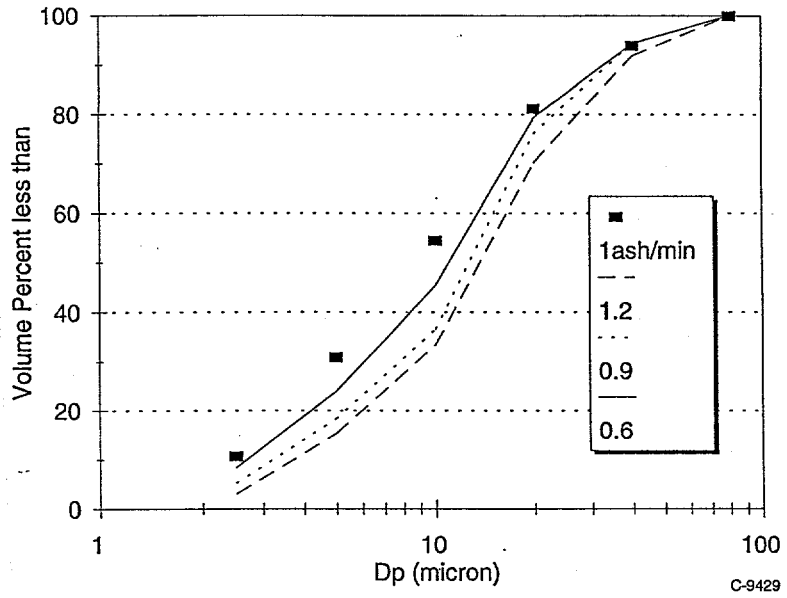

Figure 7-3. Predicted ash PSD as a function of stoichiometric ratio. Mineral size distribution (1 ash/min) shown for comparison. Coal: ROM Pittsburgh No. 8.

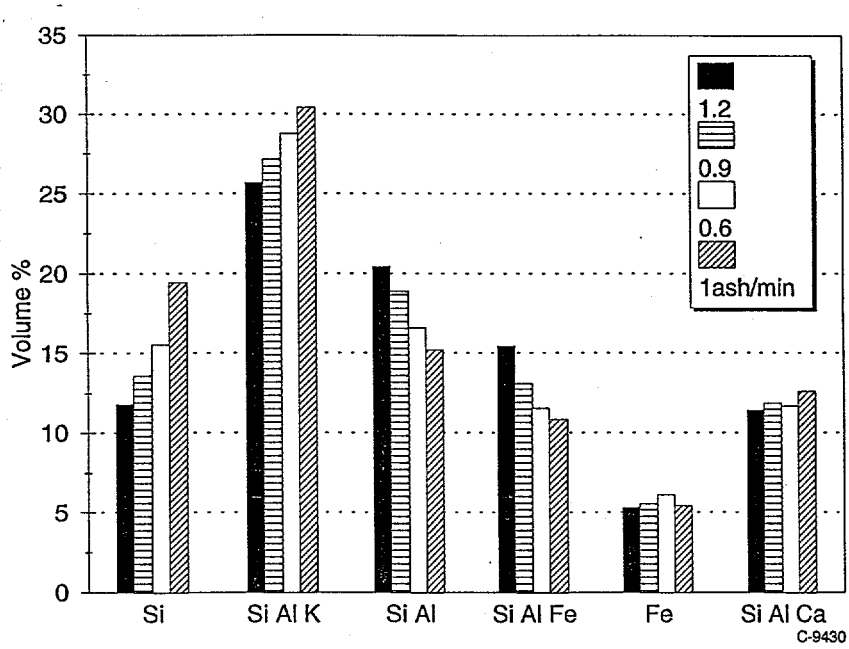

Figure 7-4. Model prediction for ash composition - ROM Pittsburgh No. 8.

References

Bool, L.E., Peterson, T.W., Wendt, J.O.L, "The Partitioning of Iron During the Combustion of Pulverized Coal.", *Comb. and Flame*, Vol 99, pp.262-270.

Dryer, F.L., and Glassman, I.; "High Temperature Oxidation of CO and CH_4"; *Fourteenth Symposium (International) on Combustion*, The Combustion Institute, Pittsburgh, PA, 1973

Groves, S.J., Williamson, J., and Sanyal, A.; "Decomposition of Pyrite During Pulverized Coal Combustion", *Fuel*, 66, 1987

Helble, J.J., et al.; "Transformations of Inorganic Coal Constituents in Combustion Systems"; Phase II Final Report, U.S. Department of Energy Contract No. DE-AC22-86PC90751, Pittsburgh Energy Technology Center, Pittsburgh, PA, 1992

Hurt, R.H. and Hardesty, D.R., "The Rates and Mechanisms of Coal Char Combustion", Coal Combustion Science Quarterly Progress Report Oct-Dec 1991, Sandia Report SAND92-8211 UC-362, 1992

Hurt, R.H., and Mitchell, R.E.; "Unified High-Temperature Char Combustion Kinetics for a Suite of Coals of Various Rank"; *The Twenty Fourth International Symposium on Combustion*; Sidney, Australia, June 5-10, 1992

Hurt, R.H, and Mitchell, R.E.; "O the Combustion Kinetics of Heterogeneous Char Particle Populations";*The Twenty Fourth International Symposium on Combustion*; Sidney, Australia, June 5-10, 1992

Westbrook, C.K., and Dryer, F.L.; "Simplified Reaction Mechanisms for the Oxidation of Hydrocarbon Fuels in Flames"; *Combust. Sci. Technol.*, 27, 1981

APPENDIX

CCSEM Data for Washed Pittsburgh #8 and Silverdale Coals

Analysis and data provided by Dr. Fraser Wigley
Imperial College, London

Data reports reproduced in their entirety

Average mineral properties for Pittsburgh pf

Average particle properties

Number	Wt %	Porosity	Shape	SiO2	Al2O3	Fe2O3	CaO	MgO	Na2O	K2O	TiO2	Mn3O4	P2O5	SO3
1268	100.00	**0.04**	**2.14**	**46.73**	**20.70**	**11.34**	**3.43**	**1.39**	**1.20**	**2.92**	**1.93**	**0.54**	**0.40**	**9.42**

Average mineral properties by chemical type

Type	*Number*	Wt %	Porosity	Shape	SiO2	Al2O3	Fe2O3	CaO	MgO	Na2O	K2O	TiO2	Mn3O4	P2O5	SO3
Alsil	*821*	59.61	0.05	2.40	55.56	31.73	3.40	0.40	1.02	0.60	3.97	0.98	0.32	0.41	1.60
Ca+Fe	*17*	4.86	0.00	1.45	0.90	0.60	25.99	52.75	12.98	0.06	0.04	0.14	2.46	0.12	3.97
Ca-alsil	*13*	0.48	0.00	2.26	20.00	9.86	2.96	29.63	0.31	0.42	0.95	0.87	0.30	3.81	30.90
Ca-rich	*10*	0.51	0.00	2.24	2.01	1.09	0.97	59.65	0.53	0.27	1.87	0.25	0.67	2.46	30.24
Fe-alsil	*74*	4.22	0.03	1.89	19.00	12.13	30.10	0.52	1.19	0.81	1.11	0.78	0.35	0.78	33.23
Fe-rich	*116*	13.20	0.01	1.60	1.18	0.64	49.36	0.26	0.32	0.88	0.16	0.15	0.28	0.19	46.59
non-CFAS	*44*	3.75	0.11	1.68	13.94	7.64	3.16	2.77	0.62	16.88	9.94	31.75	3.85	0.70	8.76
Si-rich	*173*	13.37	0.02	1.95	89.63	6.16	0.94	0.18	0.23	0.38	0.72	0.65	0.19	0.24	0.69

Average mineral properties by size

Size (µm)	*Number*	Wt %	Porosity	Shape	SiO2	Al2O3	Fe2O3	CaO	MgO	Na2O	K2O	TiO2	Mn3O4	P2O5	SO3
1 - 2	*360*	9.27	0.00	2.48	44.99	23.94	10.94	1.50	1.02	1.93	3.21	1.53	0.37	0.74	9.82
2 - 4	*214*	18.23	0.01	2.40	48.35	24.68	8.60	1.32	0.89	2.87	3.27	1.52	0.35	0.57	7.59
4 - 8	*157*	18.96	0.04	2.26	49.07	22.94	8.92	0.42	0.71	0.61	2.78	1.02	0.24	0.37	12.93
8 - 16	*433*	22.58	0.01	2.15	47.98	19.00	11.08	2.66	1.04	0.81	2.55	1.49	0.39	0.45	12.55
16 - 32	*91*	16.20	0.08	2.02	59.26	23.12	5.54	1.00	0.74	0.40	2.98	2.16	0.25	0.24	4.32
32 - 64	*12*	10.92	0.13	1.65	36.68	14.57	24.96	0.26	0.70	1.23	4.03	5.75	1.60	0.14	10.06
64 - 128	*1*	3.83	0.00	1.30	0.08	0.25	24.52	56.91	14.80	0.00	0.00	0.00	2.36	0.00	1.07

F. Wigley, Imperial College

Average mineral properties for Pittsburgh pf

Average mineral properties by chemical type and size

Type	Size (µm)	*Number*	Wt %	Porosity	Shape	SiO2	Al2O3	Fe2O3	CaO	MgO	Na2O	K2O	TiO2	Mn3O4	P2O5	SO3
Alsil	1 - 2	*246*	6.08	0.00	2.80	52.39	31.95	4.07	0.69	1.12	0.77	4.12	1.24	0.39	0.56	2.69
Alsil	2 - 4	*152*	12.71	0.02	2.58	53.22	33.02	3.82	0.42	1.04	0.55	4.07	0.75	0.30	0.46	2.35
Alsil	4 - 8	*103*	12.60	0.05	2.46	55.30	32.42	3.48	0.31	0.94	0.45	3.94	1.11	0.23	0.40	1.42
Alsil	8 - 16	*255*	12.43	0.02	2.41	56.33	31.17	3.27	0.42	1.08	0.59	4.03	1.13	0.29	0.46	1.23
Alsil	16 - 32	*59*	10.63	0.09	2.18	57.79	31.15	2.86	0.40	1.01	0.45	3.94	0.95	0.26	0.26	0.93
Alsil	32 - 64	*6*	5.16	0.19	1.79	59.27	29.22	2.82	0.16	0.94	1.24	3.57	0.60	0.73	0.30	1.15
Ca+Fe	1 - 2	*1*	0.03	0.00	1.37	4.74	3.29	25.39	23.45	0.05	0.38	0.32	0.00	0.75	0.14	41.48
Ca+Fe	2 - 4	*2*	0.32	0.00	2.01	2.56	1.71	45.70	30.07	0.39	0.07	0.16	0.95	2.97	0.64	14.77
Ca+Fe	4 - 8	*3*	0.08	0.00	2.05	8.81	5.45	20.25	31.91	3.09	0.00	0.53	1.75	3.63	0.60	23.98
Ca+Fe	8 - 16	*10*	0.59	0.00	2.05	3.98	1.41	25.58	42.48	10.10	0.42	0.15	0.39	2.69	0.52	12.28
Ca+Fe	64 - 128	*1*	3.83	0.00	1.30	0.08	0.25	24.52	56.91	14.80	0.00	0.00	0.00	2.36	0.00	1.07
Ca-alsil	1 - 2	*7*	0.16	0.00	1.82	16.59	10.84	2.02	25.07	0.31	0.44	1.45	0.83	0.41	0.55	41.49
Ca-alsil	2 - 4	*3*	0.16	0.00	3.41	16.97	12.45	1.54	27.73	0.47	0.57	0.70	0.23	0.04	8.94	30.37
Ca-alsil	8 - 16	*3*	0.16	0.00	1.54	26.65	6.17	5.38	36.33	0.15	0.26	0.68	1.56	0.44	1.94	20.43
Ca-rich	1 - 2	*2*	0.05	0.00	2.25	0.14	0.13	0.05	46.76	0.62	0.13	0.68	0.84	0.62	21.80	28.24
Ca-rich	2 - 4	*1*	0.04	0.00	2.75	3.49	2.43	0.39	34.85	0.33	0.53	0.66	0.07	1.81	0.78	54.65
Ca-rich	8 - 16	*6*	0.31	0.00	2.32	1.53	1.17	1.52	56.63	0.55	0.15	2.77	0.26	0.74	0.24	34.43
Ca-rich	16 - 32	*1*	0.11	0.00	1.76	3.72	0.74	0.00	85.07	0.50	0.61	0.23	0.00	0.00	0.50	8.62
Fe-alsil	1 - 2	*40*	1.08	0.00	1.98	22.90	16.42	29.80	0.48	1.52	1.05	1.64	1.62	0.37	0.94	23.27
Fe-alsil	2 - 4	*9*	0.93	0.00	2.05	18.33	12.78	35.31	0.98	1.88	1.05	1.18	1.20	0.35	0.87	26.07
Fe-alsil	4 - 8	*8*	1.00	0.11	1.66	13.91	10.18	29.05	0.19	0.42	0.71	0.78	0.02	0.43	0.51	43.81
Fe-alsil	8 - 16	*14*	0.75	0.00	1.96	19.34	11.21	25.85	0.61	1.45	0.70	1.06	0.48	0.17	0.88	38.26
Fe-alsil	16 - 32	*3*	0.46	0.07	1.75	21.66	6.60	29.43	0.24	0.31	0.16	0.58	0.06	0.41	0.64	39.91
Fe-rich	1 - 2	*24*	0.82	0.00	1.77	2.14	1.51	50.03	0.38	0.32	0.89	0.25	0.35	0.38	0.63	43.12
Fe-rich	2 - 4	*13*	1.31	0.00	1.74	1.18	0.81	43.73	0.28	0.26	0.64	0.36	0.28	0.21	0.32	51.92
Fe-rich	4 - 8	*14*	2.74	0.01	1.69	0.35	0.08	33.69	0.08	0.11	0.24	0.09	0.10	0.18	0.24	64.85
Fe-rich	8 - 16	*58*	3.97	0.01	1.59	1.43	0.70	42.04	0.18	0.17	0.60	0.21	0.19	0.39	0.21	53.88
Fe-rich	16 - 32	*4*	0.77	0.05	1.28	1.70	1.06	47.27	0.09	0.11	0.35	0.17	0.26	0.44	0.07	48.49
Fe-rich	32 - 64	*3*	3.57	0.01	1.52	1.21	0.63	71.88	0.50	0.71	1.87	0.05	0.02	0.22	0.00	22.90
non-CFAS	1 - 2	*13*	0.32	0.00	1.78	14.14	8.39	3.96	5.28	1.23	34.53	6.21	11.80	0.28	1.33	12.86
non-CFAS	2 - 4	*9*	0.83	0.02	1.59	11.65	5.88	1.22	1.62	0.36	51.43	5.76	18.54	0.38	0.77	2.40

F. Wigley, Imperial College

Average mineral properties by chemical type and size

Type	Size (μm)	*Number*	Wt %	Porosity	Shape	SiO2	Al2O3	Fe2O3	CaO	MgO	Na2O	K2O	TiO2	Mn3O4	P2O5	SO3
non-CFAS	4 - 8	*5*	0.12	0.00	2.35	20.55	15.32	1.11	4.48	0.54	23.07	2.54	24.35	1.24	0.56	6.25
non-CFAS	8 - 16	*11*	0.57	0.03	2.02	20.15	13.00	6.60	7.75	2.26	11.04	4.20	27.27	1.44	2.18	4.12
non-CFAS	16 - 32	*5*	0.67	0.06	2.09	28.34	17.57	8.48	3.56	0.40	0.58	4.15	34.02	0.13	0.41	2.37
non-CFAS	32 - 64	*1*	1.24	0.28	1.26	4.09	0.00	0.00	0.00	0.00	0.00	20.23	47.36	10.49	0.00	17.82
Si-rich	1 - 2	*27*	0.74	0.00	1.87	88.13	5.99	1.77	0.22	0.37	0.26	0.71	0.84	0.22	0.35	1.15
Si-rich	2 - 4	*25*	1.92	0.00	2.13	90.34	5.06	0.88	0.20	0.23	0.28	0.69	0.46	0.30	0.50	1.05
Si-rich	4 - 8	*24*	2.41	0.02	2.14	89.32	5.65	0.87	0.12	0.23	0.72	0.69	0.77	0.13	0.25	1.23
Si-rich	8 - 16	*76*	3.80	0.01	1.96	90.67	5.48	0.78	0.23	0.20	0.37	0.67	0.65	0.22	0.26	0.48
Si-rich	16 - 32	*19*	3.56	0.06	1.72	88.54	7.81	0.94	0.15	0.20	0.26	0.88	0.52	0.17	0.10	0.43
Si-rich	32 - 64	*2*	0.95	0.04	1.92	90.05	6.39	1.20	0.21	0.29	0.33	0.41	1.07	0.00	0.00	0.03

Particle properties:

Type - Assigned using the following scheme

non-CFAS - (CaO + Fe2O3 + Al2O3 + SiO2) < 80 wt%, otherwise

Si-rich - SiO2' > 80 wt%

Fe-rich - Fe2O3' > 80 wt%

Ca-rich - CaO' > 80 wt%

Alsil - (Al2O3' + SiO2') > 80 wt% and SiO2' < 80 wt%

Ca-alsil - (Al2O3' + SiO2') < 80 wt% and CaO' < 80 wt% and Fe2O3' < 20 wt% and CaO' > Fe2O3'

Fe-alsil - (Al2O3' + SiO2') < 80 wt% and Fe2O3' < 80 wt% and CaO' < 20 wt% and Fe2O3' > CaO'

Ca+Fe - CaO' > 20 wt% and Fe2O3' > 20 wt%

where CaO', Fe2O3', Al2O3' and SiO2' are normalised to (CaO' + Fe2O3' + Al2O3' + SiO2')=100%.

Size - The diameter of a circle with the same area as the analysed cross-section of the particle.

Number - Number of particles analysed.

Wt% - Mass percentage of particles analysed, using an estimated density.

Porosity - Area fraction of pores seen in cross-section (should be treated with caution).

Shape - Aspect ratio of particle cross-section (should be treated with caution).

Viscosity - Estimated using the scheme of Kalmanovitch and Frank (1988) (takes no account of the physical state of the phase, and should be treated with caution).

F. Wigley, Imperial College

Average mineral properties for Pittsburgh pf

Number of minerals by size and chemical type

Size (μm)	Fe-rich	Fe-alsil	Alsil	Ca-alsil	Ca-rich	Si-rich	Ca+Fe	non-CFAS
1 - 2	24	40	246	7	2	27	1	13
2 - 4	13	9	152	3	1	25	2	9
4 - 8	14	8	103			24	3	5
8 - 16	58	14	255	3	6	76	10	11
16 - 32	4	3	59		1	19		5
32 - 64	3		6			2		1
64 - 128							1	

Mass abundance (wt%) of minerals by size and chemical type

Size (μm)	Fe-rich	Fe-alsil	Alsil	Ca-alsil	Ca-rich	Si-rich	Ca+Fe	non-CFAS
1 - 2	0.82	1.08	6.08	0.16	0.05	0.74	0.03	0.32
2 - 4	1.31	0.93	12.71	0.16	0.04	1.92	0.32	0.83
4 - 8	2.74	1.00	12.60			2.41	0.08	0.12
8 - 16	3.97	0.75	12.43	0.16	0.31	3.80	0.59	0.57
16 - 32	0.77	0.46	10.63		0.11	3.56		0.67
32 - 64	3.57		5.16			0.95		1.24
64 - 128							3.83	

Average porosity of minerals by size and chemical type

Size (μm)	Fe-rich	Fe-alsil	Alsil	Ca-alsil	Ca-rich	Si-rich	Ca+Fe	non-CFAS
1 - 2	0.00	0.00	0.00	0.00	0.00	0.00	0.00	0.00
2 - 4	0.00	0.00	0.02	0.00	0.00	0.00	0.00	0.02
4 - 8	0.01	0.11	0.05			0.02	0.00	0.00
8 - 16	0.01	0.00	0.02	0.00	0.00	0.01	0.00	0.03
16 - 32	0.05	0.07	0.09		0.00	0.06		0.06
32 - 64	0.01		0.19			0.04		0.28
64 - 128							0.00	

Average shape of minerals by size and chemical type

Size (μm)	Fe-rich	Fe-alsil	Alsil	Ca-alsil	Ca-rich	Si-rich	Ca+Fe	non-CFAS
1 - 2	1.77	1.98	2.80	1.82	2.25	1.87	1.37	1.78
2 - 4	1.74	2.05	2.58	3.41	2.75	2.13	2.01	1.59
4 - 8	1.69	1.66	2.46			2.14	2.05	2.35
8 - 16	1.59	1.96	2.41	1.54	2.32	1.96	2.05	2.02
16 - 32	1.28	1.75	2.18		1.76	1.72		2.09
32 - 64	1.52		1.79			1.92		1.26
64 - 128							1.30	

F. Wigley, Imperial College

Mineral size distribution for Pittsburgh pf

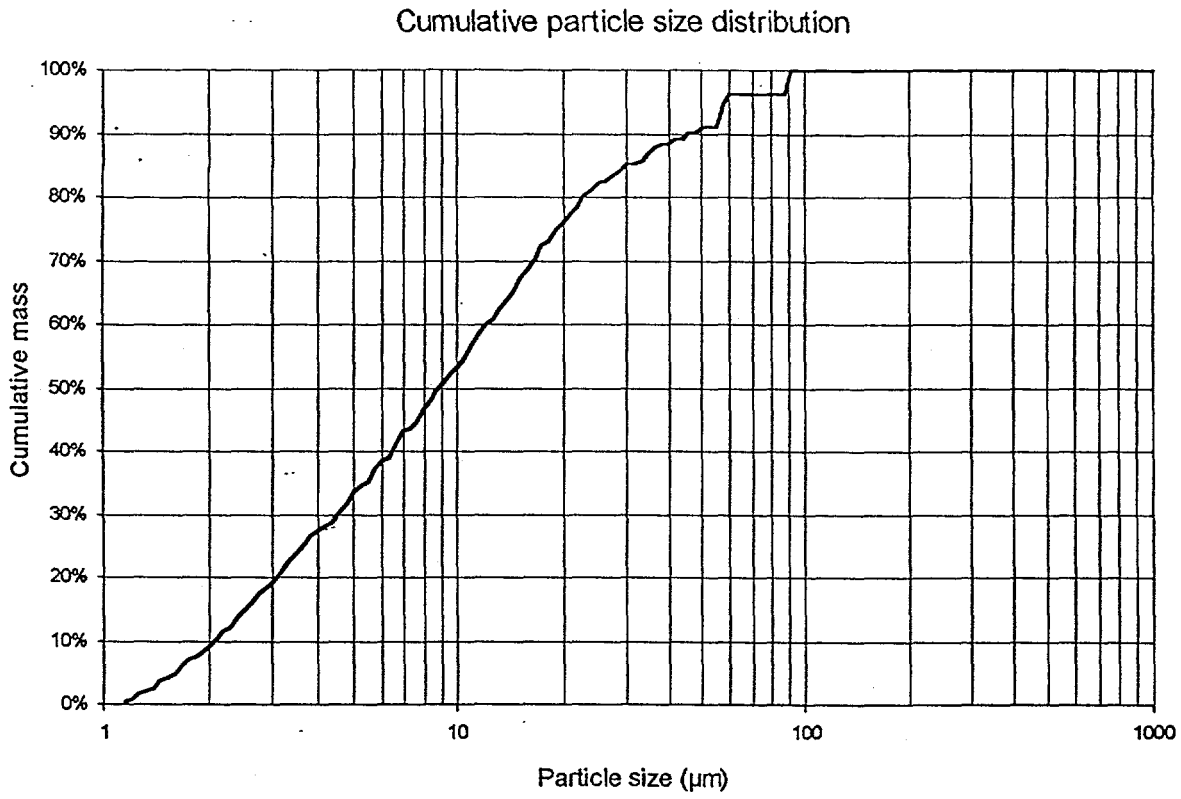

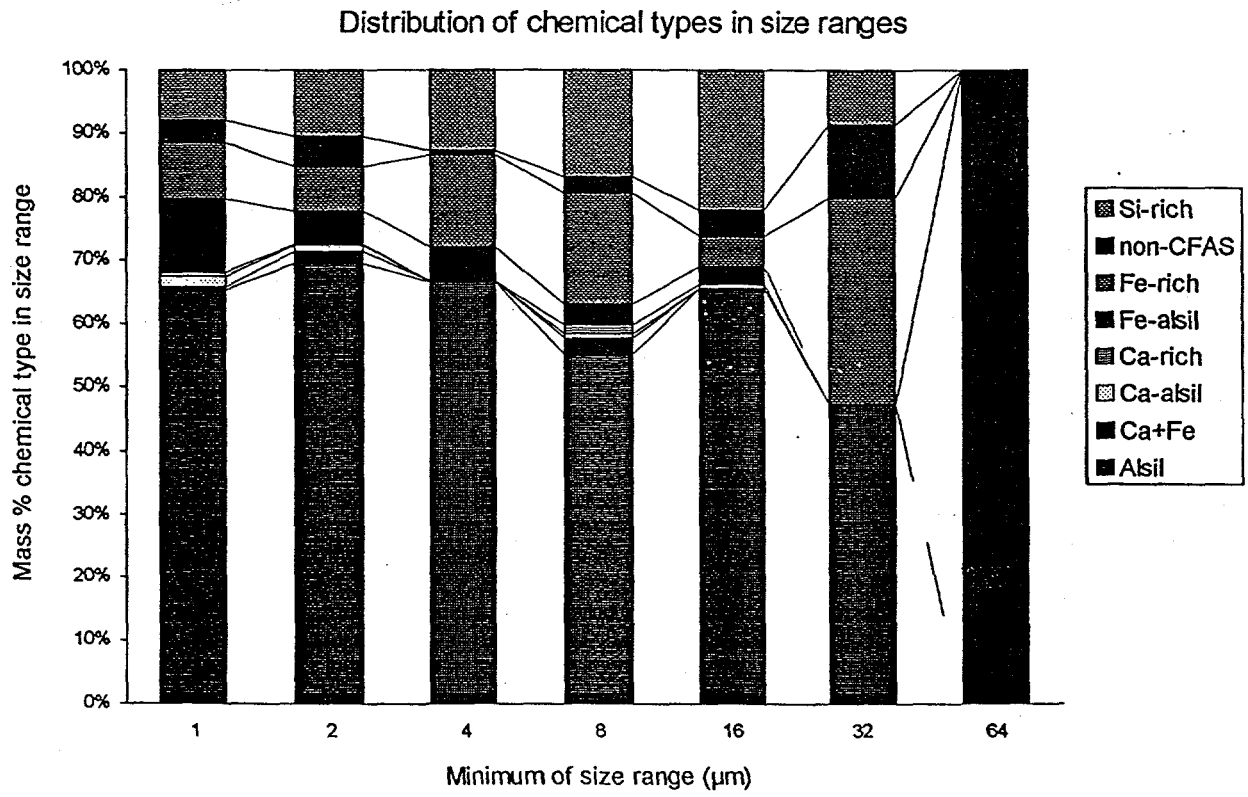

F. Wigley, Imperial College

Mineral chemical distribution for Pittsburgh pf

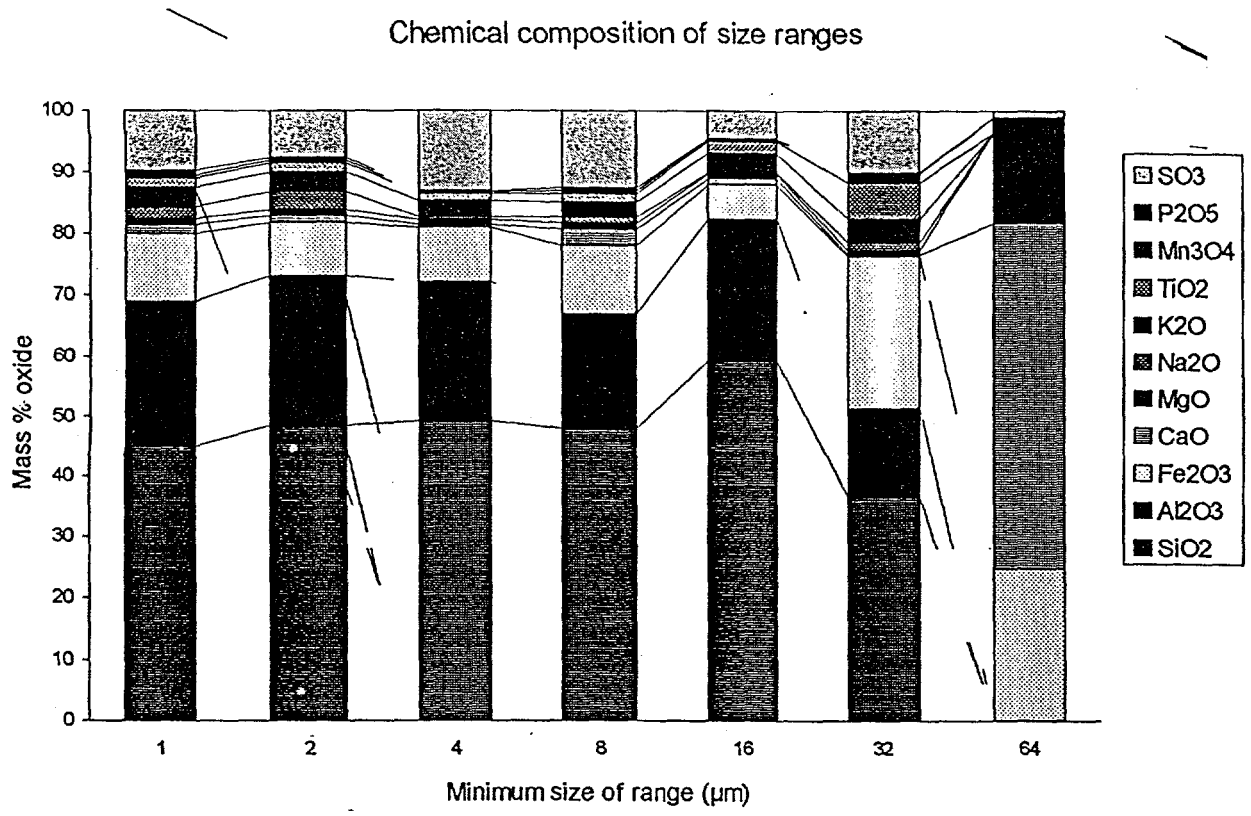

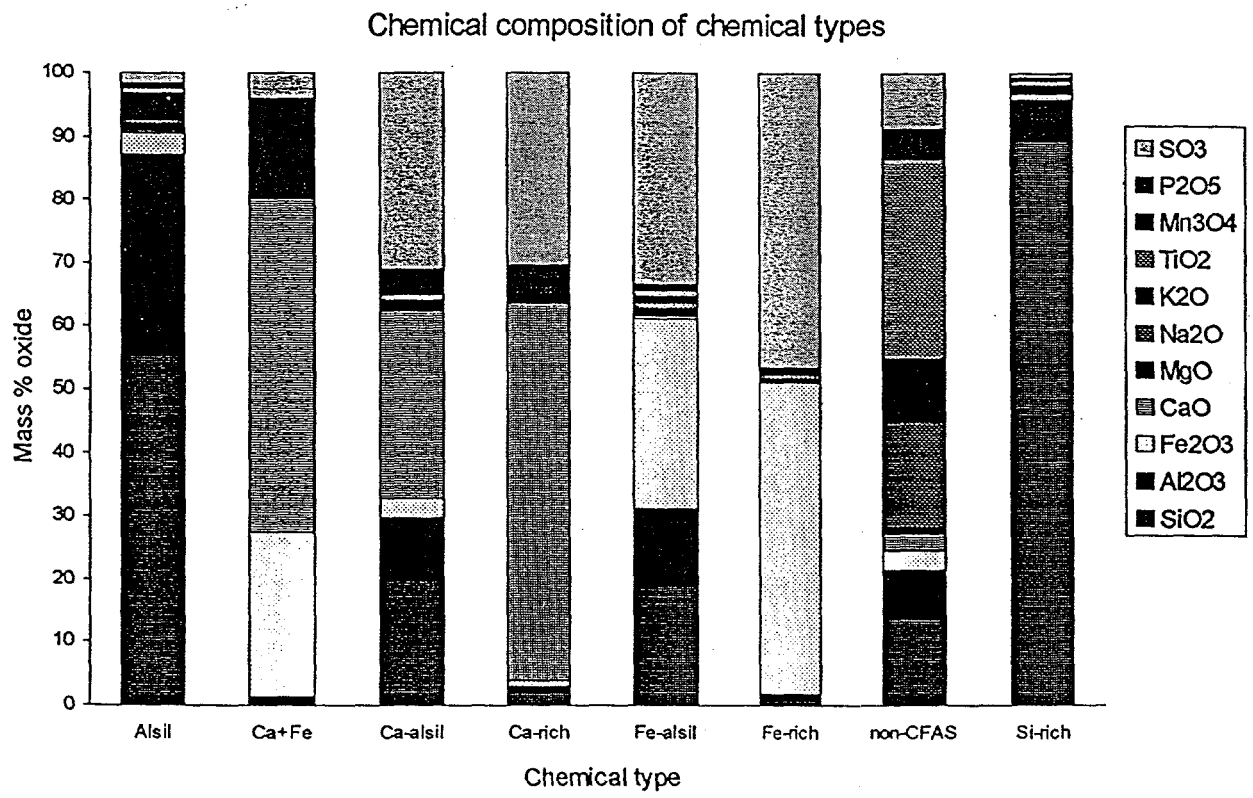

F. Wigley, Imperial College

Particle viscosity distribution for minerals in Pittsburgh pf

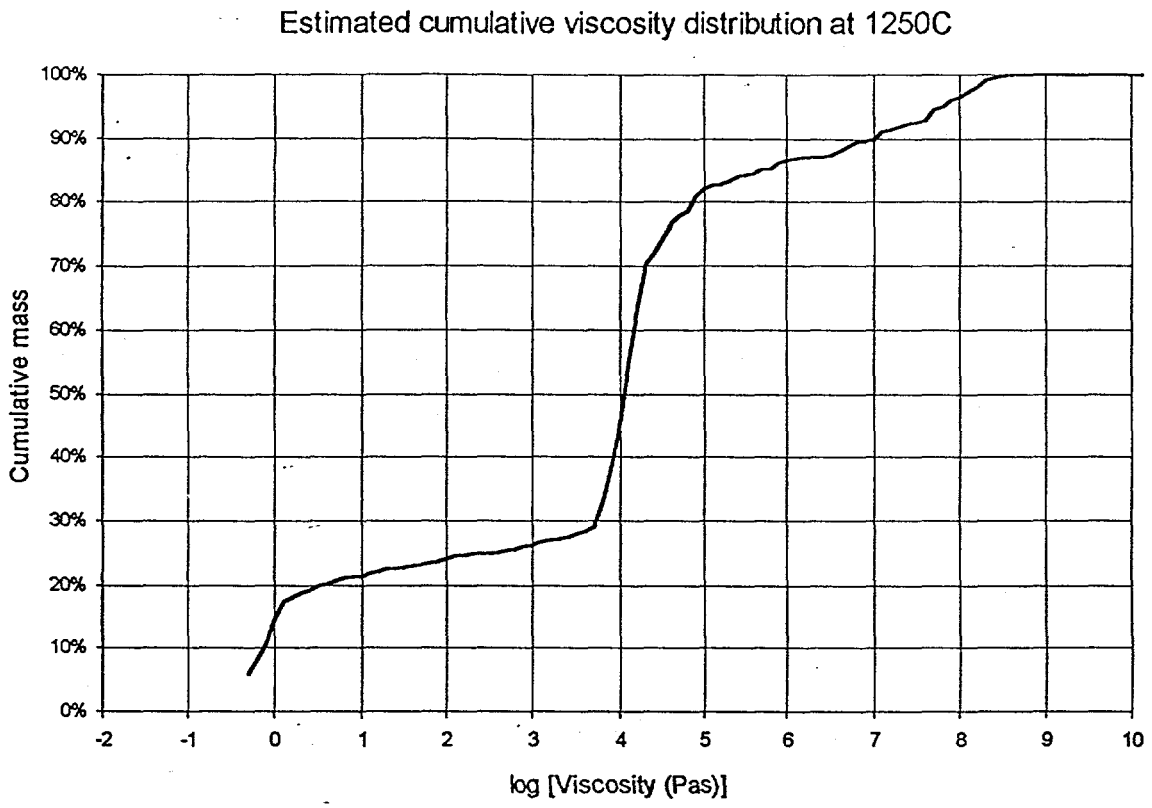

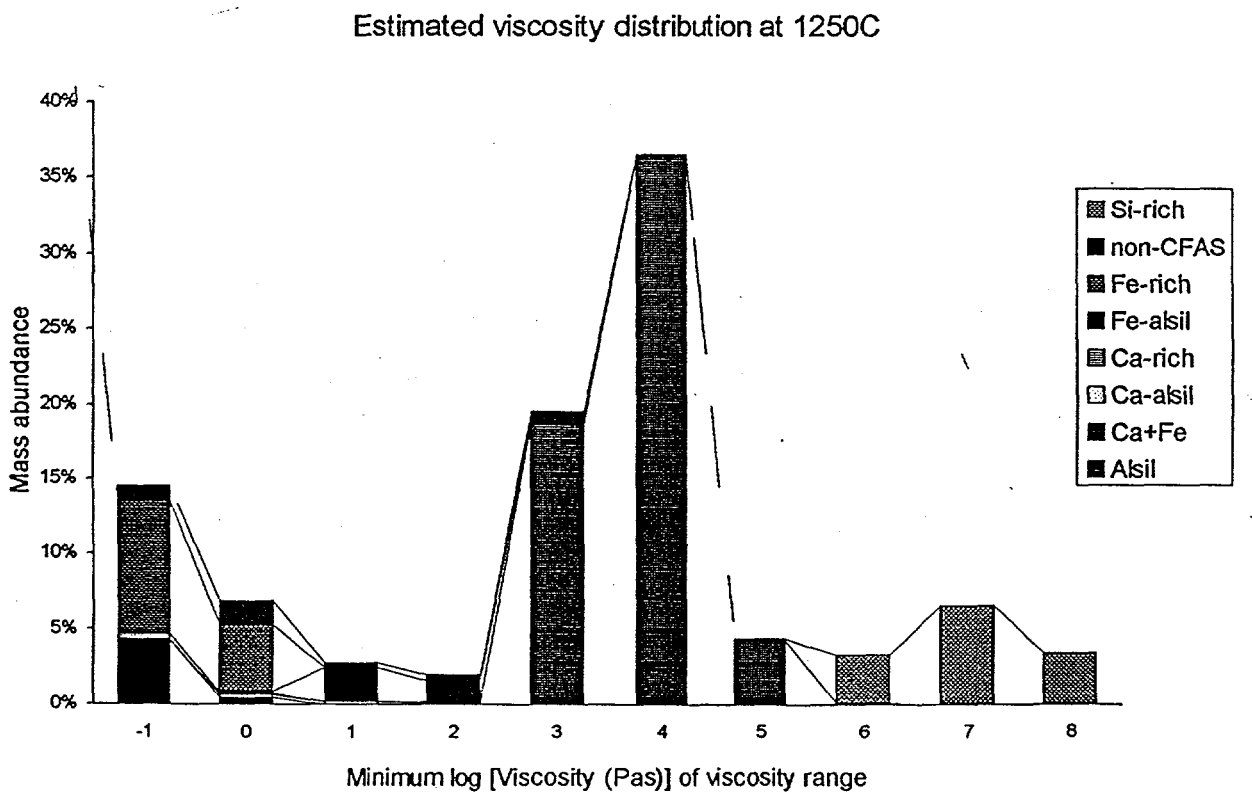

F. Wigley, Imperial College

Ternary diagrams for minerals in Pittsburgh pf

Fe_2O_3 - Al_2O_3 - SiO_2

for Si-rich, Alsil, Fe-alsil, Fe-rich and Ca+Fe chemical types

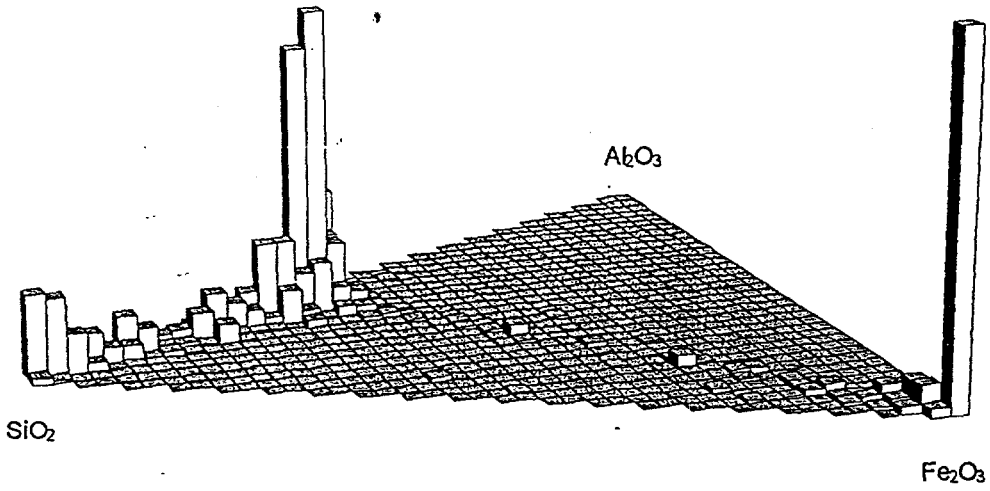

CaO - Al_2O_3 - SiO_2

for Si-rich, Alsil, Ca-alsil, Ca-rich and Ca+Fe chemical types

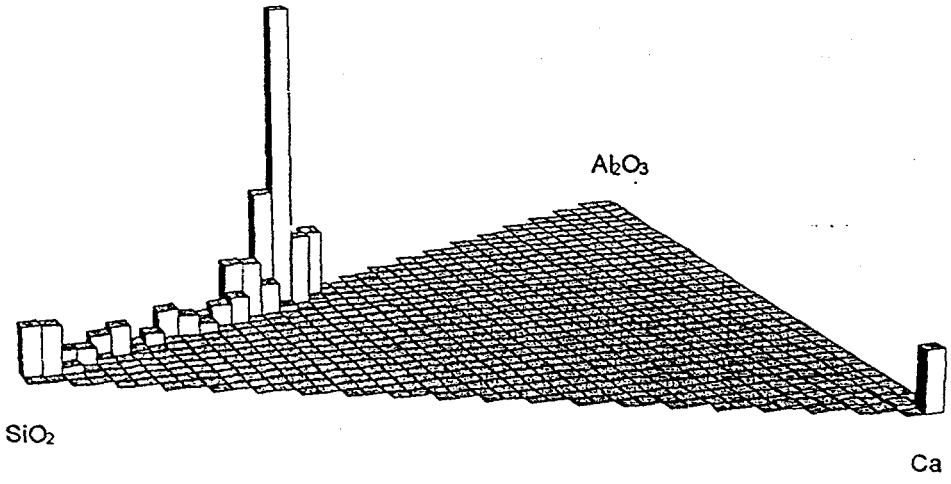

F. Wigley, Imperial College

Ternary diagrams for minerals in Pittsburgh pf

$CaO - Fe_2O_3 - (Al_2O_3 + SiO_2)$

for all chemical types except non-CFA

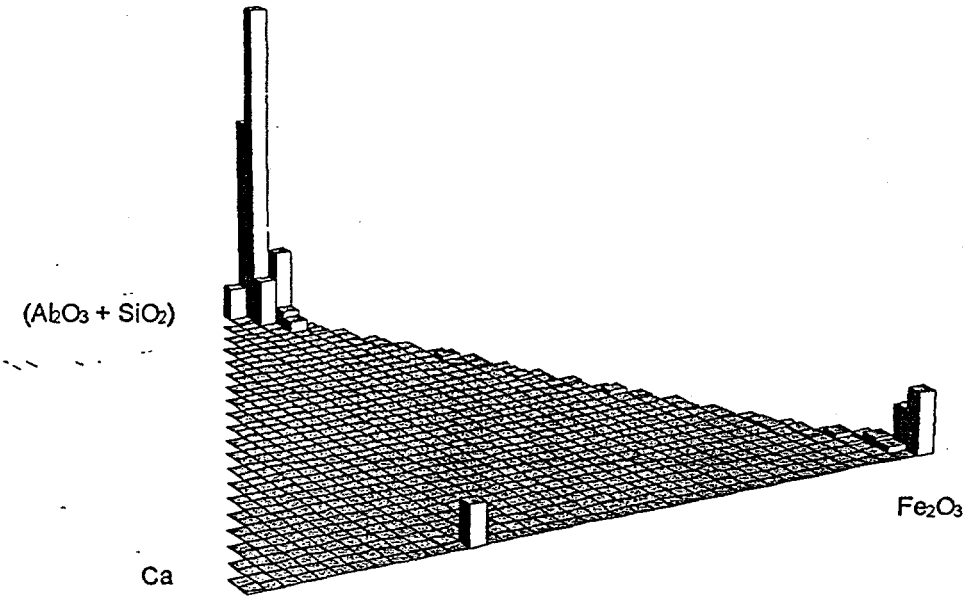

$10*K_2O - Al_2O_3 - SiO_2$

for Alsil and Si-rich chemical types

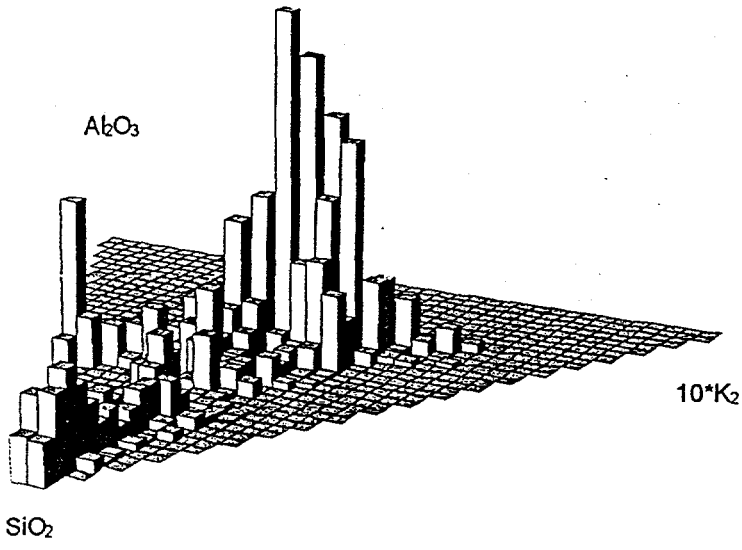

F. Wigley, Imperial College

$Na_2O - K_2O - CaO$

where $(Na_2O+K_2O+CaO) > 1wt\%$

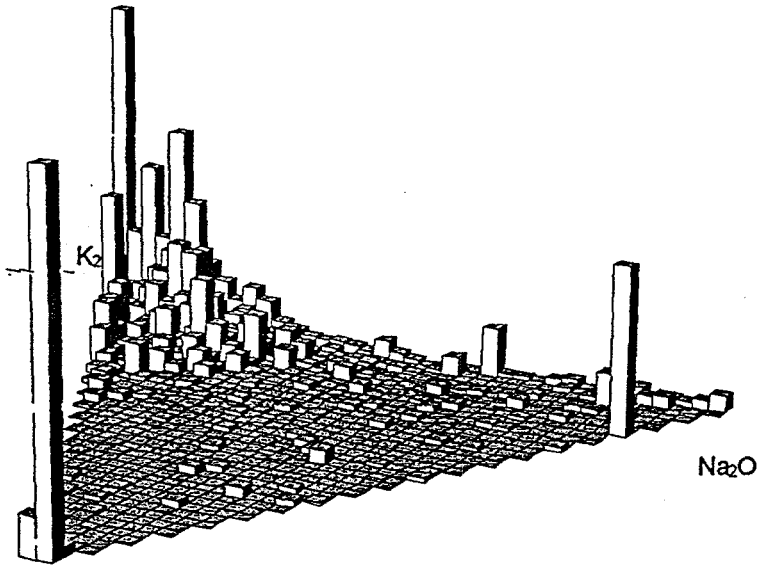

$MgO - Fe_2O_3 - CaO$

where $(MgO+Fe_2O_3+CaO) > 20wt\%$

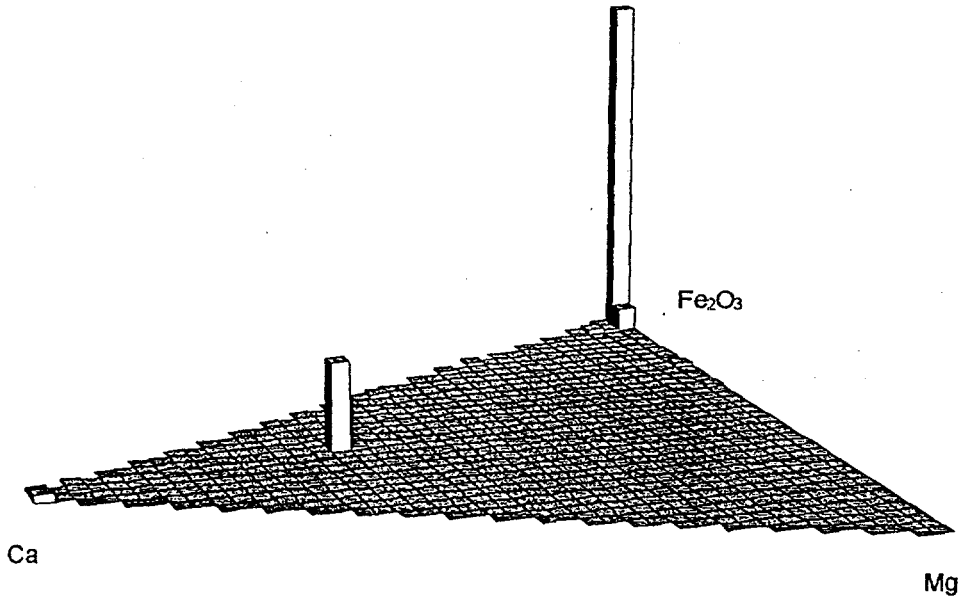

F. Wigley, Imperial College

Fe - S - O

for Fe-alsil, Fe-rich, Ca+Fe and non-CFAS chemical type

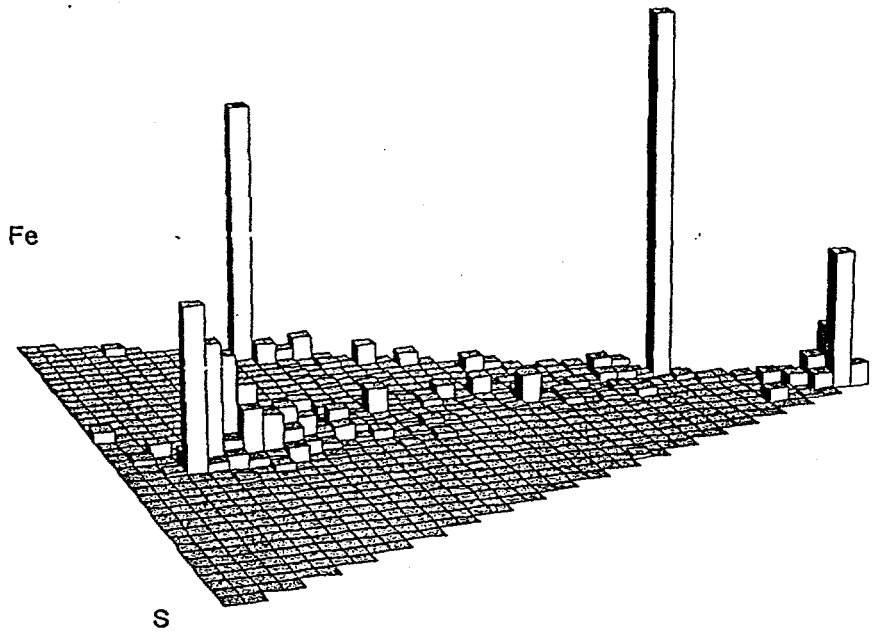

Ca - S - O

for Ca-alsil, Ca-rich, Ca+Fe and non-CFAS chemical type

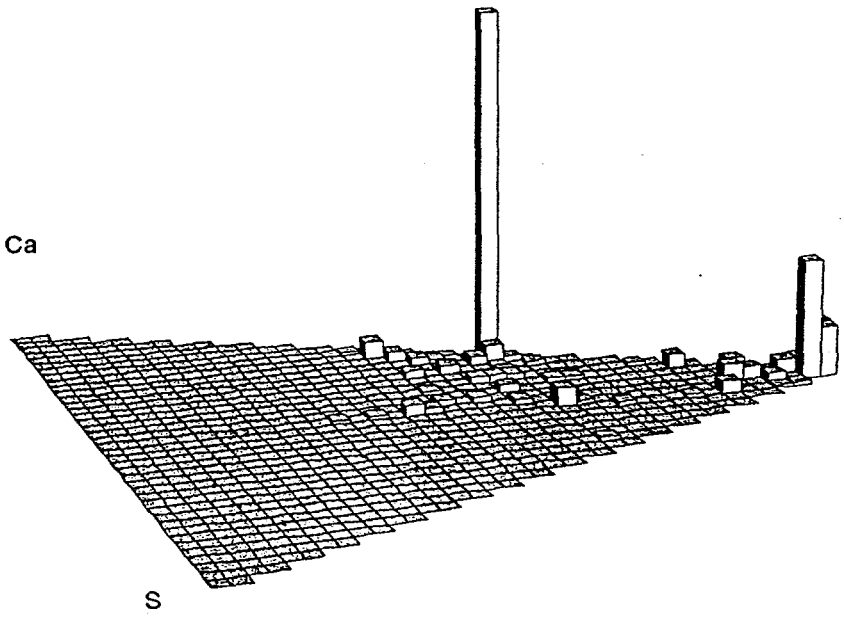

F. Wigley, Imperial College

Average mineral properties for Silverdale pf

Average particle properties

	Number	Wt %	Porosity	Shape	SiO2	Al2O3	Fe2O3	CaO	MgO	Na2O	K2O	TiO2	Mn3O4	P2O5	SO3
	1139	100.00	**0.02**	**2.03**	**36.33**	**18.04**	**13.64**	**3.44**	**0.66**	**0.64**	**1.35**	**1.22**	**0.38**	**0.48**	**23.80**

Average mineral properties by chemical type

Type	*Number*	Wt %	Porosity	Shape	SiO2	Al2O3	Fe2O3	CaO	MgO	Na2O	K2O	TiO2	Mn3O4	P2O5	SO3
Alsil	*590*	48.56	0.04	2.34	56.38	33.72	2.29	0.46	0.51	0.47	2.43	0.94	0.29	0.51	2.01
Ca+Fe	*4*	0.38	0.02	2.07	3.32	1.86	23.70	44.39	9.77	0.27	0.23	0.31	4.27	0.68	11.22
Ca-alsil	*11*	0.72	0.03	1.62	16.42	5.78	5.32	35.03	0.27	0.20	0.55	0.51	0.63	2.60	32.68
Ca-rich	*28*	3.05	0.01	2.21	1.65	0.82	1.01	59.37	0.26	0.24	0.18	0.22	0.44	1.49	34.31
Fe-alsil	*100*	8.08	0.02	1.84	14.73	10.01	29.60	0.75	0.56	0.44	0.58	0.40	0.66	0.52	41.74
Fe-rich	*277*	27.65	0.01	1.63	0.92	0.65	33.74	0.30	0.12	0.27	0.11	0.17	0.36	0.18	63.19
non-CFAS	*36*	3.71	0.05	1.76	9.06	2.62	15.23	22.28	7.40	7.40	0.81	17.17	1.01	1.29	15.73
Si-rich	*93*	7.85	0.01	1.89	89.04	6.45	1.05	0.17	0.22	0.25	0.74	0.53	0.19	0.39	0.98

Average mineral properties by size

Size (µm)	*Number*	Wt %	Porosity	Shape	SiO2	Al2O3	Fe2O3	CaO	MgO	Na2O	K2O	TiO2	Mn3O4	P2O5	SO3
1 - 2	*401*	11.77	0.00	2.28	35.25	19.28	14.00	1.16	0.48	0.64	1.42	1.51	0.38	0.70	25.17
2 - 4	*180*	17.53	0.00	2.32	43.01	22.87	9.34	2.70	0.69	1.28	1.52	1.26	0.36	0.67	16.30
4 - 8	*122*	18.19	0.03	1.87	37.63	16.77	15.24	4.27	1.18	0.57	1.37	2.63	0.43	0.39	19.51
8 - 16	*337*	21.73	0.01	2.06	29.68	14.60	15.83	4.35	0.65	0.59	1.24	0.89	0.47	0.55	31.14
16 - 32	*84*	20.12	0.04	1.87	36.69	19.19	14.02	4.08	0.51	0.43	1.38	0.59	0.40	0.34	22.38
32 - 64	*15*	10.65	0.06	1.83	37.15	15.74	12.38	2.66	0.28	0.21	1.16	0.32	0.13	0.25	29.71

F. Wigley, Imperial College

Average mineral properties for Silverdale pf

Average mineral properties by chemical type and size

Type	Size (µm)	*Number*	Wt %	Porosity	Shape	SiO2	Al2O3	Fe2O3	CaO	MgO	Na2O	K2O	TiO2	Mn3O4	P2O5	SO3
Alsil	1 - 2	*219*	5.98	0.00	2.78	53.13	34.43	2.75	0.59	0.55	0.58	2.39	1.21	0.39	0.69	3.29
Alsil	2 - 4	*118*	10.55	0.00	2.53	54.85	35.20	2.24	0.46	0.41	0.54	2.19	0.86	0.34	0.49	2.42
Alsil	4 - 8	*58*	8.36	0.04	2.20	55.96	33.23	2.83	0.24	0.61	0.41	2.58	0.73	0.23	0.38	2.80
Alsil	8 - 16	*144*	8.50	0.02	2.54	57.11	32.61	2.07	0.47	0.55	0.61	2.68	1.23	0.34	0.67	1.66
Alsil	16 - 32	*44*	10.58	0.07	2.07	58.94	32.68	2.05	0.48	0.46	0.37	2.36	0.93	0.23	0.39	1.10
Alsil	32 - 64	*7*	4.59	0.13	1.81	57.60	34.79	1.74	0.59	0.55	0.26	2.41	0.58	0.24	0.54	0.70
Ca+Fe	1 - 2	*1*	0.03	0.00	2.03	2.85	1.74	19.60	14.28	0.00	0.67	0.38	1.00	0.19	0.24	59.05
Ca+Fe	4 - 8	*1*	0.03	0.24	1.60	13.86	10.79	17.41	29.60	7.82	0.00	1.77	0.00	0.00	1.57	17.17
Ca+Fe	8 - 16	*1*	0.12	0.00	2.17	2.45	0.59	24.67	47.60	10.30	0.00	0.00	0.16	6.38	0.73	7.12
Ca+Fe	16 - 32	*1*	0.20	0.00	2.08	2.28	1.27	24.71	49.33	11.24	0.40	0.11	0.34	4.30	0.58	5.45
Ca-alsil	1 - 2	*1*	0.02	0.00	3.42	7.05	4.92	1.42	34.01	0.11	0.00	0.83	0.90	0.00	0.98	49.77
Ca-alsil	2 - 4	*3*	0.39	0.00	1.43	14.72	5.10	3.72	28.53	0.14	0.10	0.39	0.65	0.42	2.06	44.20
Ca-alsil	4 - 8	*3*	0.09	0.00	1.78	16.29	13.04	4.94	39.60	1.41	0.27	1.03	0.20	0.86	10.05	12.31
Ca-alsil	8 - 16	*4*	0.22	0.08	1.71	20.25	4.15	8.60	44.62	0.07	0.38	0.62	0.36	0.96	0.71	19.27
Ca-rich	1 - 2	*4*	0.10	0.00	2.35	1.28	1.75	2.38	50.88	0.00	0.69	0.12	0.54	0.37	6.08	35.90
Ca-rich	2 - 4	*3*	0.22	0.00	2.35	2.50	1.34	1.53	41.24	0.33	0.04	0.11	0.00	0.04	8.82	44.05
Ca-rich	4 - 8	*3*	0.48	0.00	1.84	1.06	0.77	2.59	58.03	0.58	0.00	0.22	0.47	0.59	0.08	35.61
Ca-rich	8 - 16	*13*	0.81	0.00	2.00	1.74	0.97	1.08	70.85	0.37	0.33	0.22	0.45	0.77	2.02	21.19
Ca-rich	16 - 32	*4*	0.75	0.02	1.37	2.63	1.16	0.53	74.50	0.20	0.00	0.11	0.05	0.51	0.36	19.95
Ca-rich	32 - 64	*1*	0.69	0.00	3.55	0.68	0.00	0.00	37.33	0.00	0.54	0.23	0.00	0.00	0.00	61.22
Fe-alsil	1 - 2	*38*	1.16	0.00	1.74	12.35	9.16	25.49	0.72	0.38	0.68	0.55	0.64	0.33	0.83	48.87
Fe-alsil	2 - 4	*7*	0.77	0.00	2.43	14.12	11.63	22.67	1.05	0.27	0.25	0.70	0.40	0.11	0.97	47.84
Fe-alsil	4 - 8	*11*	0.91	0.00	1.61	8.37	6.37	28.30	0.57	0.08	0.57	0.21	0.47	0.16	0.19	54.72
Fe-alsil	8 - 16	*33*	2.11	0.01	1.96	12.66	8.99	28.21	0.73	0.65	0.49	0.47	0.51	0.60	0.52	46.16
Fe-alsil	16 - 32	*11*	3.13	0.06	1.71	18.99	11.67	34.13	0.75	0.78	0.32	0.75	0.23	1.11	0.40	30.88
Fe-rich	1 - 2	*94*	3.34	0.00	1.69	1.31	0.85	34.63	0.33	0.10	0.51	0.18	0.56	0.41	0.20	60.91
Fe-rich	2 - 4	*24*	3.06	0.00	2.01	1.28	1.16	35.65	0.54	0.10	0.46	0.15	0.23	0.42	0.15	59.86
Fe-rich	4 - 8	*27*	4.42	0.00	1.57	1.24	0.82	42.03	0.89	0.12	0.26	0.14	0.14	0.98	0.31	53.08
Fe-rich	8 - 16	*106*	8.04	0.01	1.60	0.87	0.66	31.31	0.16	0.20	0.20	0.09	0.14	0.28	0.17	65.92
Fe-rich	16 - 32	*21*	4.81	0.00	1.36	0.57	0.35	30.68	0.08	0.04	0.20	0.03	0.07	0.13	0.18	67.67
Fe-rich	32 - 64	*5*	3.98	0.01	1.70	0.46	0.22	30.94	0.01	0.06	0.13	0.12	0.00	0.05	0.05	67.96

F. Wigley, Imperial College

Average mineral properties by chemical type and size

Type	Size (μm)	*Number*	Wt %	Porosity	Shape	SiO2	Al2O3	Fe2O3	CaO	MgO	Na2O	K2O	TiO2	Mn3O4	P2O5	SO3
non-CFAS	1 - 2	*12*	0.28	0.00	1.70	10.44	8.20	4.92	6.18	4.46	4.19	1.37	24.29	0.45	4.39	31.11
non-CFAS	2 - 4	*5*	0.78	0.04	1.68	4.10	1.31	11.46	24.65	8.35	18.86	1.43	13.90	1.08	1.62	13.23
non-CFAS	4 - 8	*8*	1.83	0.07	1.44	8.02	1.35	20.70	21.27	7.98	2.56	0.32	21.86	0.43	0.46	15.05
non-CFAS	8 - 16	*10*	0.68	0.00	1.84	15.39	5.78	12.34	21.30	7.06	6.45	1.37	7.92	2.96	2.12	17.31
non-CFAS	16 - 32	*1*	0.14	0.04	5.97	16.45	0.00	0.00	58.77	2.21	17.79	0.00	4.78	0.00	0.00	0.00
Si-rich	1 - 2	*32*	0.86	0.00	2.04	87.11	5.79	1.28	0.36	0.31	0.31	0.87	1.08	0.31	0.72	1.87
Si-rich	2 - 4	*20*	1.75	0.00	2.00	86.03	7.71	1.60	0.26	0.31	0.27	0.74	0.53	0.22	0.71	1.63
Si-rich	4 - 8	*11*	2.08	0.01	1.64	89.74	6.55	1.05	0.11	0.23	0.30	0.81	0.26	0.13	0.29	0.54
Si-rich	8 - 16	*26*	1.25	0.00	2.06	87.15	8.09	0.85	0.21	0.17	0.21	1.01	0.64	0.20	0.40	1.07
Si-rich	16 - 32	*2*	0.51	0.00	3.10	94.70	2.38	0.90	0.12	0.08	0.30	0.40	0.34	0.35	0.17	0.26
Si-rich	32 - 64	*2*	1.39	0.03	1.44	92.61	5.15	0.46	0.00	0.15	0.11	0.44	0.55	0.10	0.00	0.42

Particle properties:

Type - Assigned using the following scheme

non-CFAS - (CaO + Fe2O3 + Al2O3 + SiO2) < 80 wt%, otherwise
Si-rich - SiO2' > 80 wt%
Fe-rich - Fe2O3' > 80 wt%
Ca-rich - CaO' > 80 wt%
Alsil - (Al2O3' + SiO2') > 80 wt% and SiO2' < 80 wt%
Ca-alsil - (Al2O3' + SiO2') < 80 wt% and CaO' < 80 wt% and Fe2O3' < 20 wt% and CaO' > Fe2O3'
Fe-alsil - (Al2O3' + SiO2') < 80 wt% and Fe2O3' < 80 wt% and CaO' < 20 wt% and Fe2O3' > CaO'
Ca+Fe - CaO' > 20 wt% and Fe2O3' > 20 wt%

where CaO', Fe2O3', Al2O3' and SiO2' are normalised to (CaO' + Fe2O3' + Al2O3' + SiO2')=100%.

Size - The diameter of a circle with the same area as the analysed cross-section of the particle.
Number - Number of particles analysed.
Wt% - Mass percentage of particles analysed, using an estimated density.
Porosity - Area fraction of pores seen in cross-section (should be treated with caution).
Shape - Aspect ratio of particle cross-section (should be treated with caution).
Viscosity - Estimated using the scheme of Kalmanovitch and Frank (1988) (takes no account of the physical state of the phase, and should be treated with caution).

F. Wigley, Imperial College

Average mineral properties for Silverdale pf

Number of minerals by size and chemical type

Size (µm)	Fe-rich	Fe-alsil	Alsil	Ca-alsil	Ca-rich	Si-rich	Ca+Fe	non-CFAS
1 - 2	94	38	219	1	4	32	1	12
2 - 4	24	7	118	3	3	20		5
4 - 8	27	11	58	3	3	11	1	8
8 - 16	106	33	144	4	13	26	1	10
16 - 32	21	11	44		4	2	1	1
32 - 64	5		7		1	2		

Mass abundance (wt%) of minerals by size and chemical type

Size (µm)	Fe-rich	Fe-alsil	Alsil	Ca-alsil	Ca-rich	Si-rich	Ca+Fe	non-CFAS
1 - 2	3.34	1.16	5.98	0.02	0.10	0.86	0.03	0.28
2 - 4	3.06	0.77	10.55	0.39	0.22	1.75		0.78
4 - 8	4.42	0.91	8.36	0.09	0.48	2.08	0.03	1.83
8 - 16	8.04	2.11	8.50	0.22	0.81	1.25	0.12	0.68
16 - 32	4.81	3.13	10.58		0.75	0.51	0.20	0.14
32 - 64	3.98		4.59		0.69	1.39		

Average porosity of minerals by size and chemical type

Size (µm)	Fe-rich	Fe-alsil	Alsil	Ca-alsil	Ca-rich	Si-rich	Ca+Fe	non-CFAS
1 - 2	0.00	0.00	0.00	0.00	0.00	0.00	0.00	0.00
2 - 4	0.00	0.00	0.00	0.00	0.00	0.00		0.04
4 - 8	0.00	0.00	0.04	0.00	0.00	0.01	0.24	0.07
8 - 16	0.01	0.01	0.02	0.08	0.00	0.00	0.00	0.00
16 - 32	0.00	0.06	0.07		0.02	0.00	0.00	0.04
32 - 64	0.01		0.13		0.00	0.03		

Average shape of minerals by size and chemical type

Size (µm)	Fe-rich	Fe-alsil	Alsil	Ca-alsil	Ca-rich	Si-rich	Ca+Fe	non-CFAS
1 - 2	1.69	1.74	2.78	3.42	2.35	2.04	2.03	1.70
2 - 4	2.01	2.43	2.53	1.43	2.35	2.00		1.68
4 - 8	1.57	1.61	2.20	1.78	1.84	1.64	1.60	1.44
8 - 16	1.60	1.96	2.54	1.71	2.00	2.06	2.17	1.84
16 - 32	1.36	1.71	2.07		1.37	3.10	2.08	5.97
32 - 64	1.70		1.81		3.55	1.44		

F. Wigley, Imperial College

Mineral size distribution for Silverdale pf

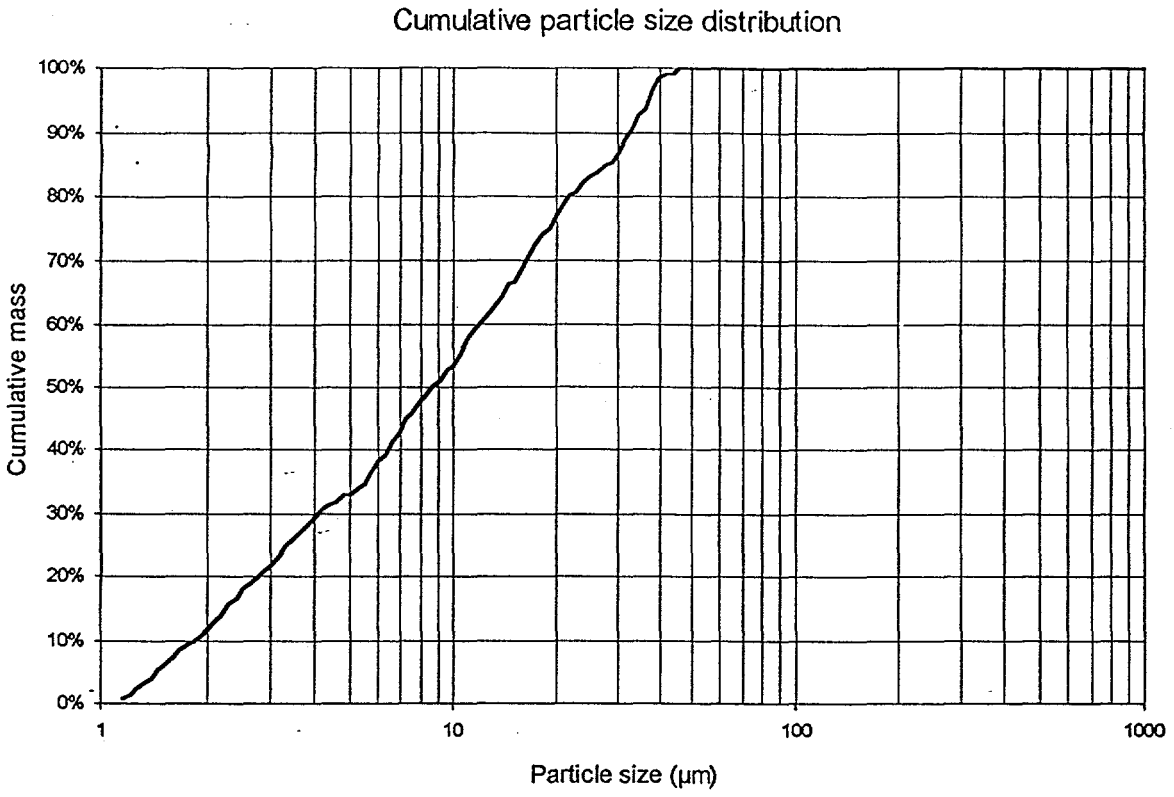

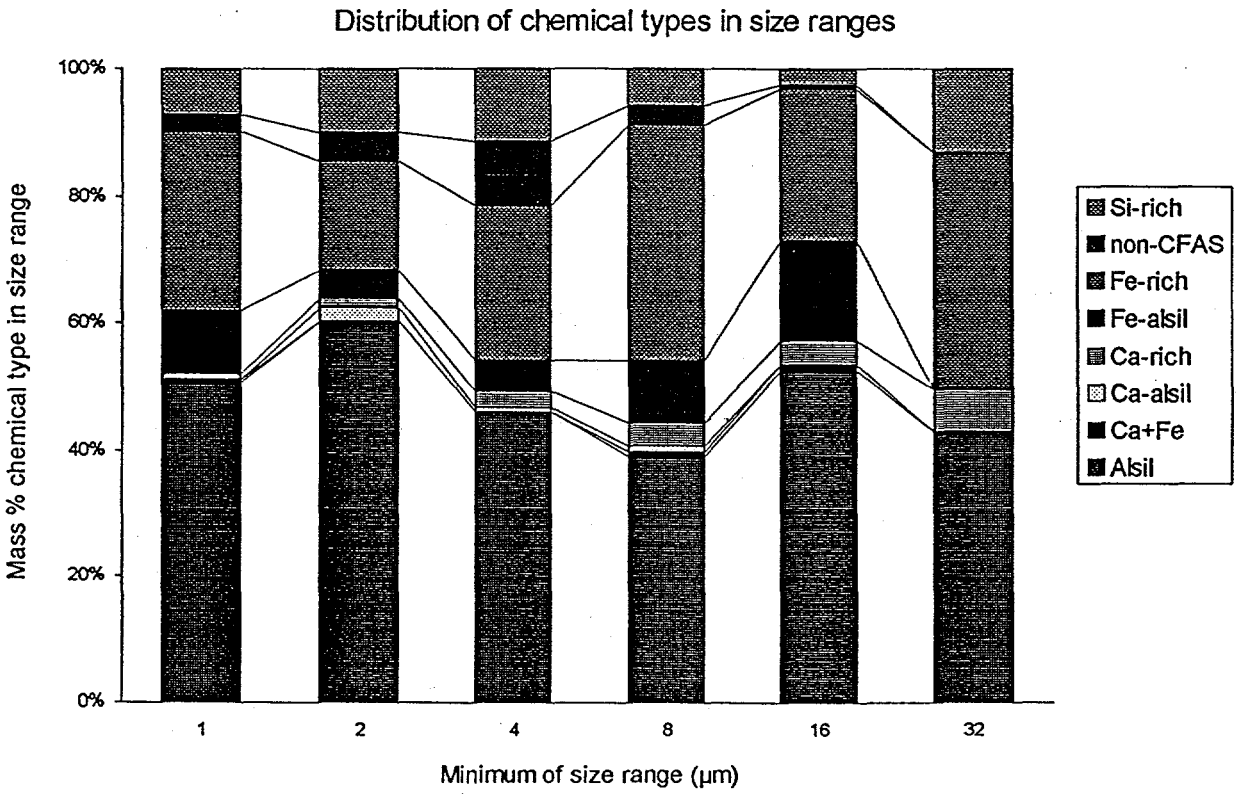

F. Wigley, Imperial College

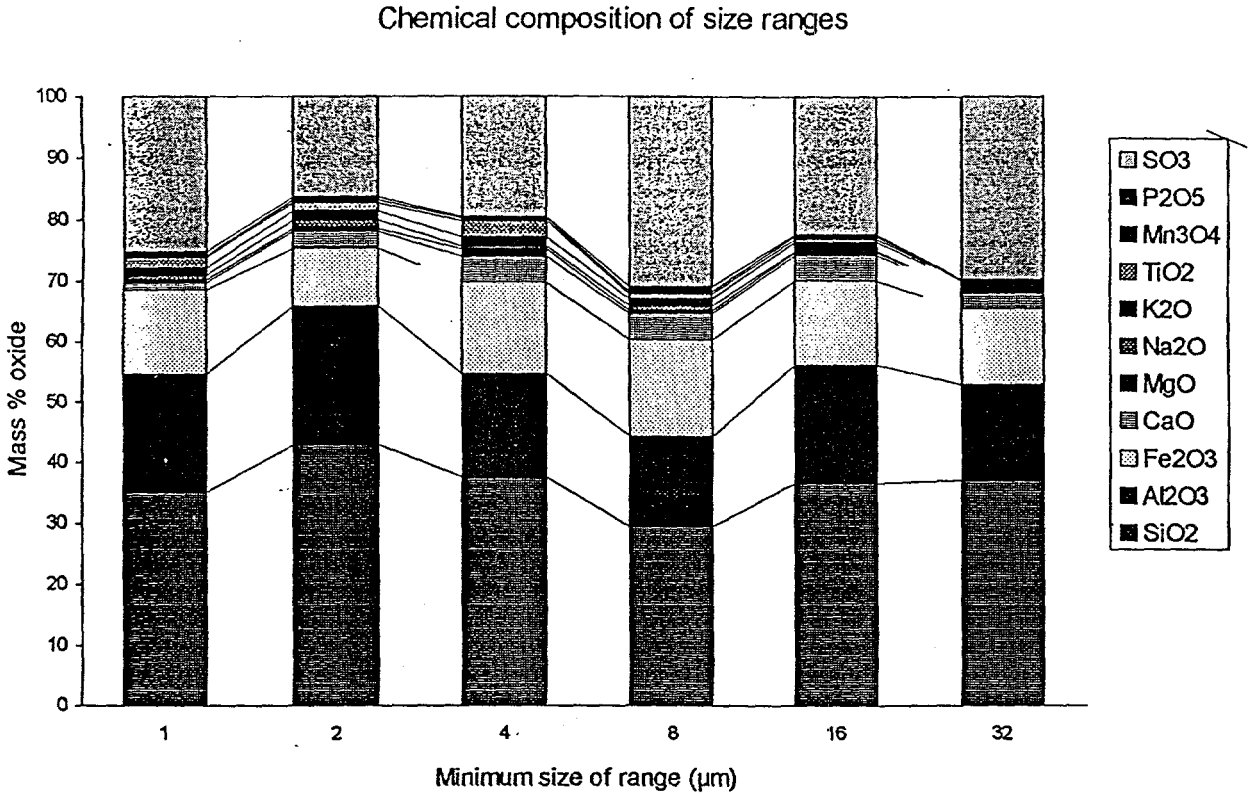

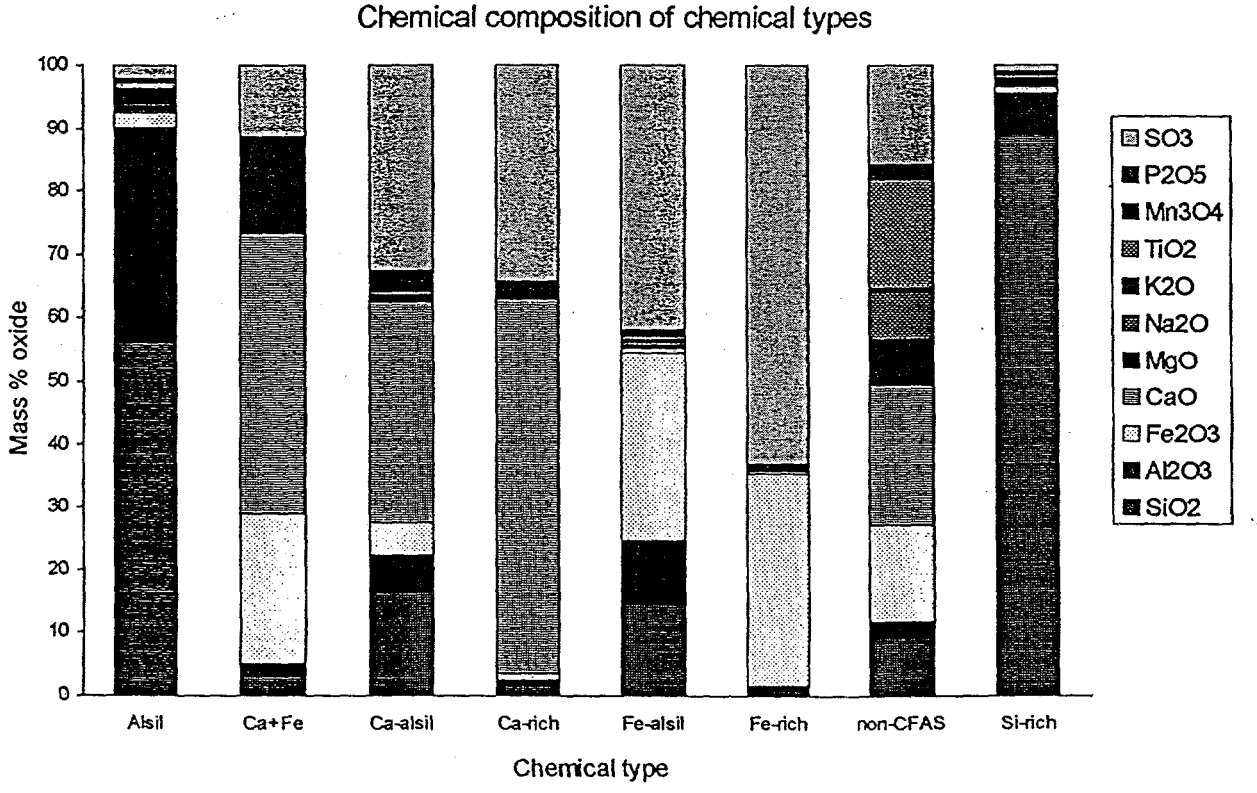

F. Wigley, Imperial College

Particle viscosity distribution for minerals in Silverdale pf

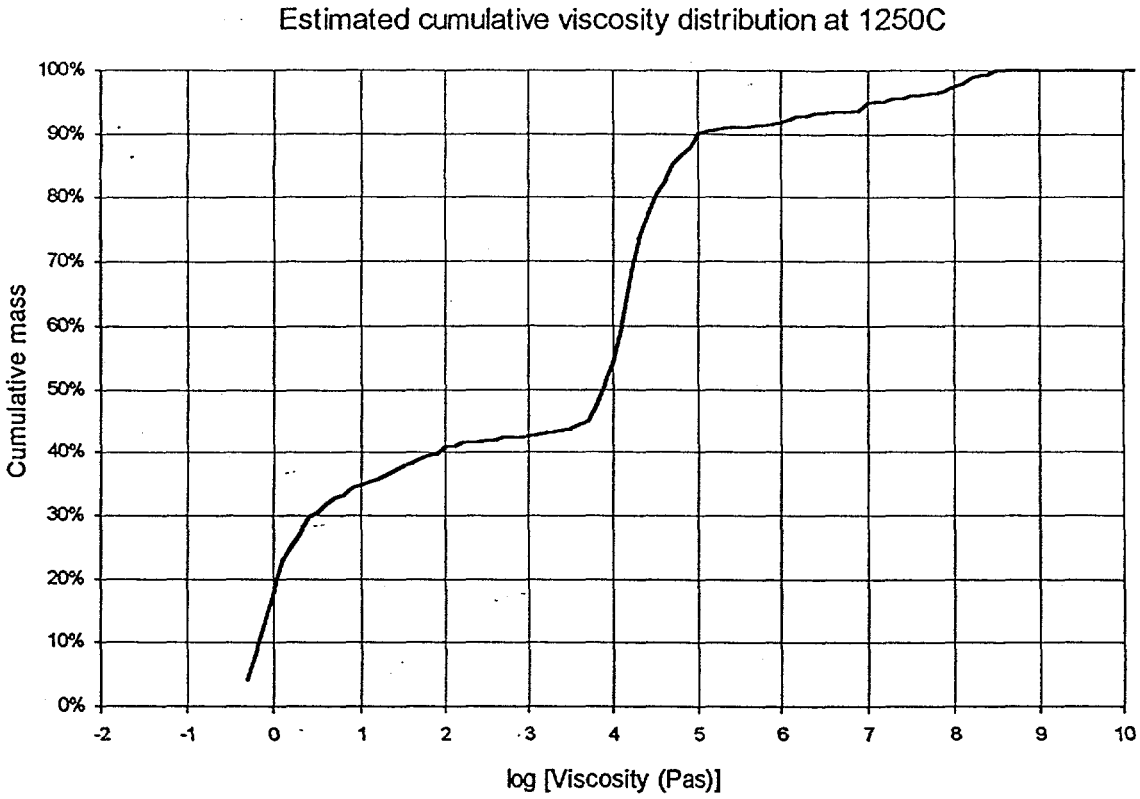

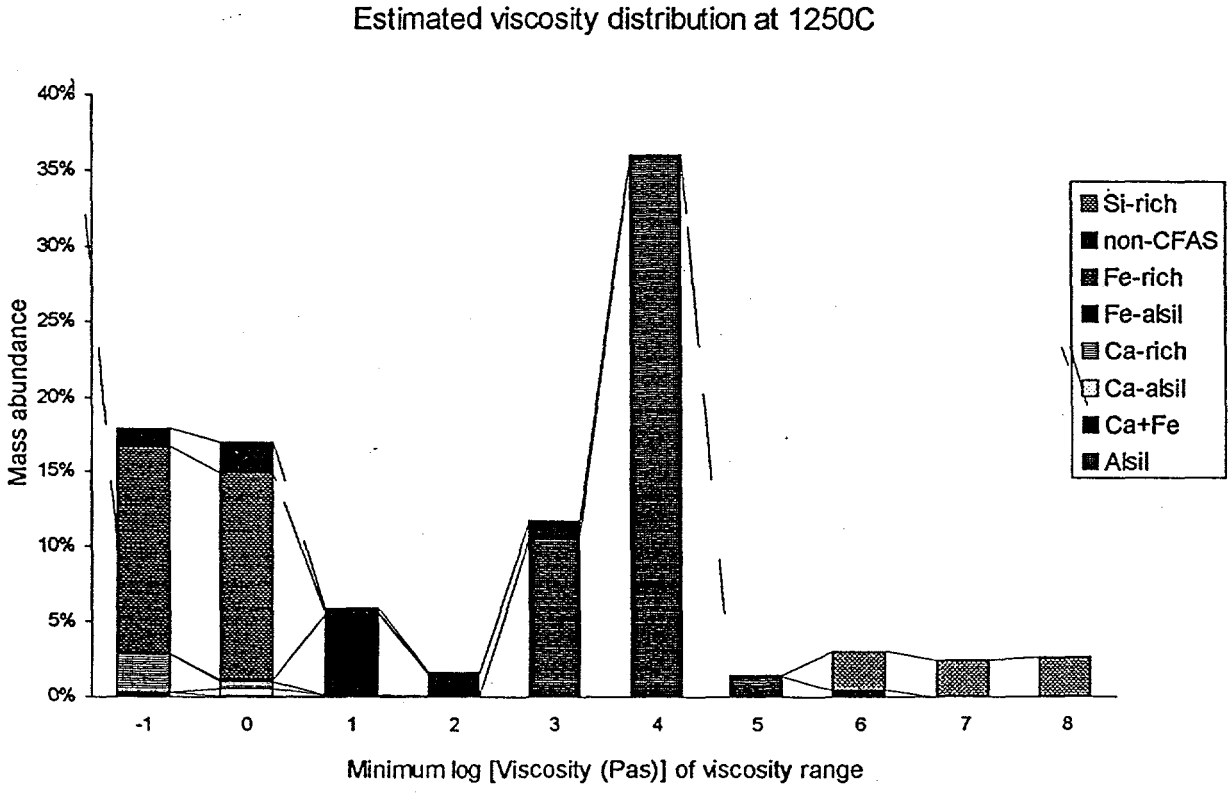

F. Wigley, Imperial College

$Fe_2O_3 - Al_2O_3 - SiO_2$

for Si-rich, Alsil, Fe-alsil, Fe-rich and Ca+Fe chemical types

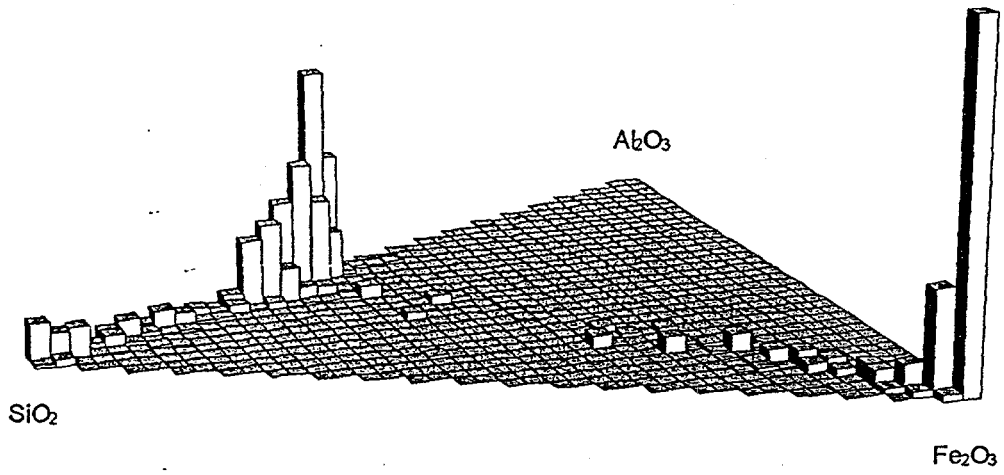

$CaO - Al_2O_3 - SiO_2$

for Si-rich, Alsil, Ca-alsil, Ca-rich and Ca+Fe chemical types

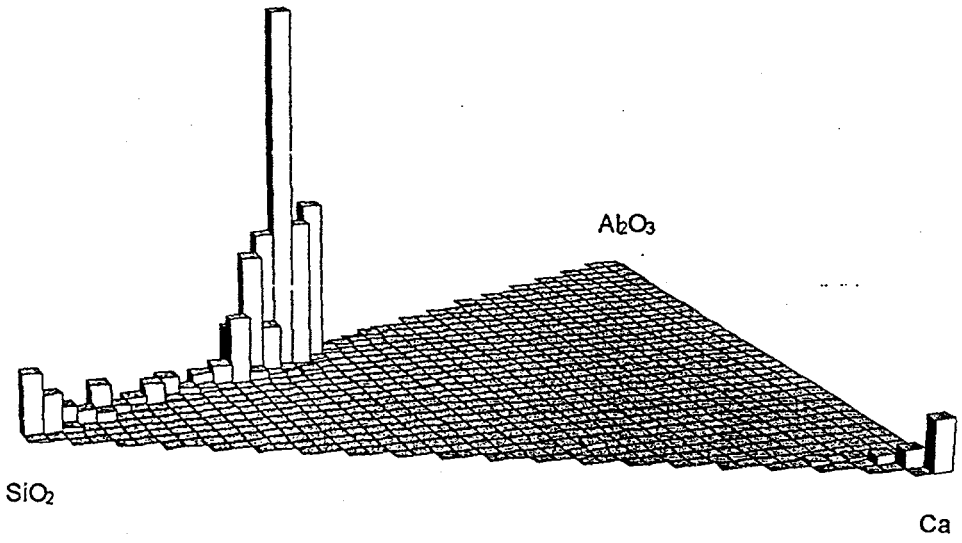

F. Wigley, Imperial College

$CaO - Fe_2O_3 - (Al_2O_3 + SiO_2)$

for all chemical types except non-CFA

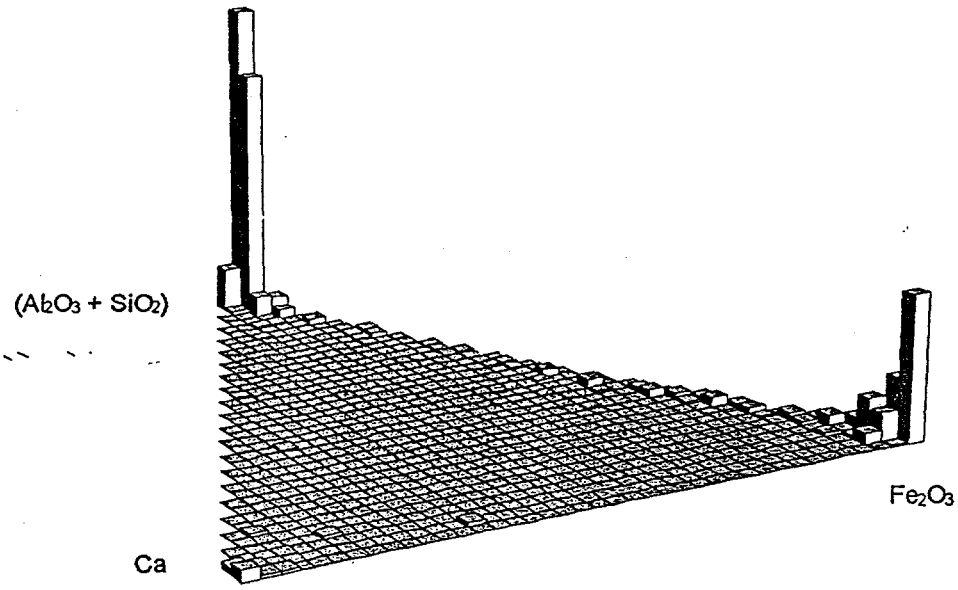

$10*K_2O - Al_2O_3 - SiO_2$

for Alsil and Si-rich chemical types

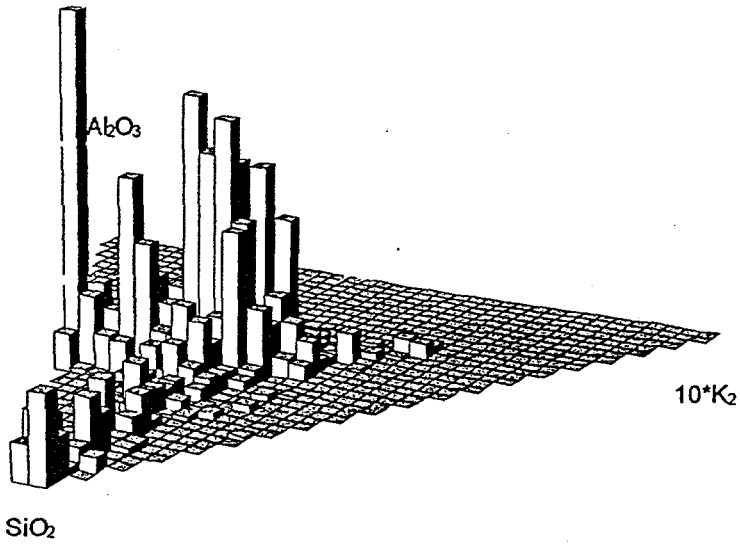

F. Wigley, Imperial College

Ternary diagram for minerals in Silverdale pf

$Na_2O - K_2O - CaO$

where $(Na_2O+K_2O+CaO) > 1wt\%$

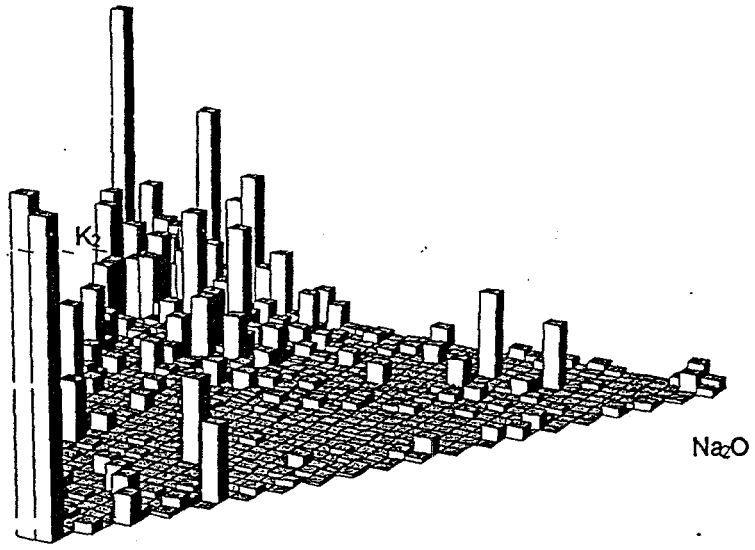

$MgO - Fe_2O_3 - CaO$

where $(MgO+Fe_2O_3+CaO) > 20wt\%$

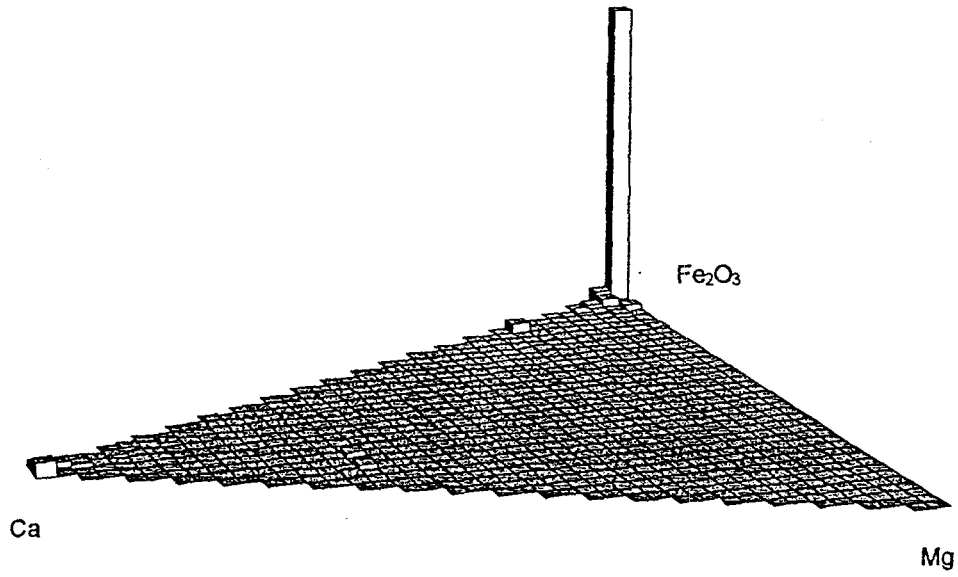

F. Wigley, Imperial College

Ternary diagrams for minerals in Silverdale pf

Fe - S - O

for Fe-alsil, Fe-rich, Ca+Fe and non-CFAS chemical type

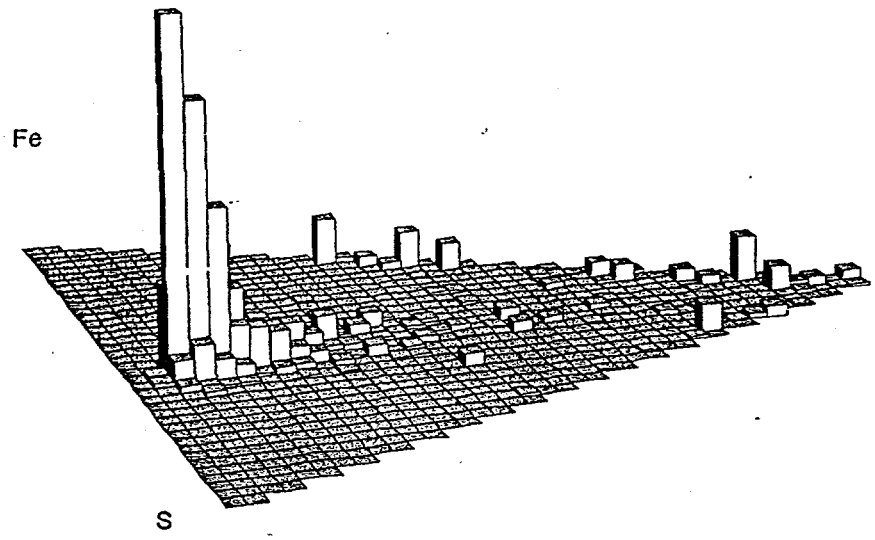

Ca - S - O

for Ca-alsil, Ca-rich, Ca+Fe and non-CFAS chemical type

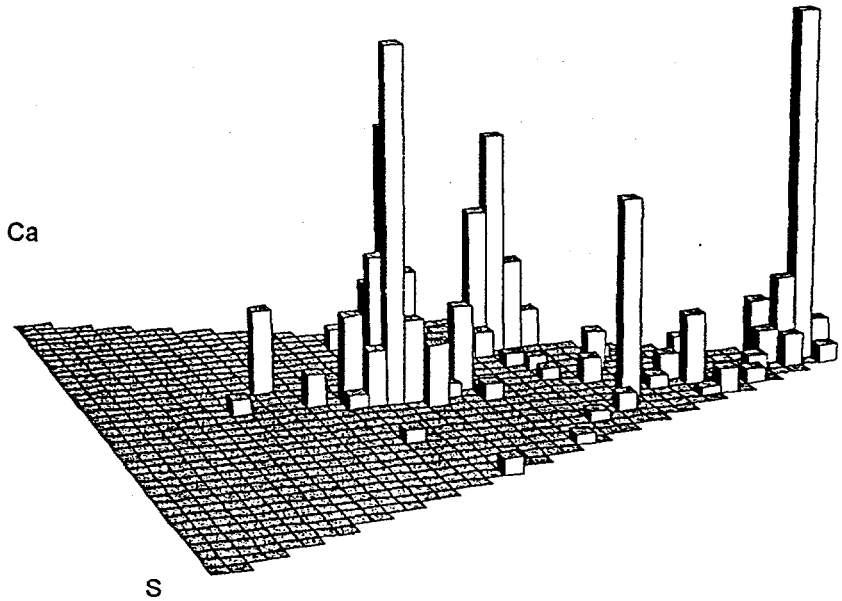

F. Wigley, Imperial College